Mon. Not. R. Astron. Soc. **000**, 1–xxx (2008) Printed 19 February 2009 (MN LATEX style file v2.2)

The Structure of Molecular Clouds: I - All Sky Near Infrared Extinction Maps

Jonathan Rowles [1⋆] Dirk Froebrich [1]†
[1]*Centre for Astrophysics & Planetary Science, The University of Kent, Canterbury, Kent CT2 7NH, U.K.*

Accepted ..... Received ..... ; in original form .....

ABSTRACT

We are studying the column density distribution of all nearby giant molecular clouds. As part of this project we generated several all sky extinction maps. They are calculated using the *median* near infrared colour excess technique applied to data from the Two Micron All-Sky Survey (2MASS). Our large scale approach allows us to fit spline functions to extinction free regions in order to accurately determine the colour excess values. Two types of maps are presented: i) Maps with a constant noise and variable spatial resolution; ii) Maps with a constant spatial resolution and variable noise. Our *standard* A_V map uses the nearest 49 stars to the centre of each pixel for the determination of the extinction. The one sigma variance is constant at 0.28 mag A_V in the entire map. The distance to the 49^{th} nearest star varies from below $1'$ near the Galactic Plane to about $10'$ at the poles, but is below $5'$ for all giant molecular clouds ($|b| < 30^\circ$). A comparison with existing large scale maps shows that our extinction values are systematically larger by 20 % compared to Dobashi et al. and 40 % smaller compared to Schlegel et al.. This is most likely caused by the applied star counting technique in Dobashi et al. and systematic uncertainties in the dust temperature and emissivity in Schlegel et al.. Our superior resolution allows us to detect more small scale high extinction cores compared to the other two maps.

Key words: star formation – extinction – ISM: clouds – ISM: dust – ISM: molecules

1 INTRODUCTION

Stars form within giant molecular clouds (GMCs). A large fraction of these stars originate in embedded clusters (Lada & Lada (2003)). The properties of these forming clusters, such as the mass function and the star formation efficiency, are hence inextricably linked to the properties of their natal molecular cloud. Of particular importance is the turbulence within the clouds. Thus, the study of the dynamics, structure and chemistry of GMCs plays a pivotal role in our understanding of the star formation process.

In order to study the turbulence within GMCs we can investigate their column density distribution and compare it to theoretical predictions for the volume density distribution which is found to be log-normal for isothermal flows (e.g. Passot & Vázquez-Semadeni (1998) and references therein). For a large number of clouds along the line of sight with a log-normal volume density distribution the column density distribution becomes normal. Otherwise the column density distribution is log-normal (Vázquez-Semadeni & García (2001)).

There are in principle a variety of ways in which the column density distribution of GMCs can be investigated. These include e.g. thermal continuum imaging of the cold dust, spectral line mapping of molecules such as CO, or the determination of extinction maps. Each of these methods has its own shortcomings, considering the accuracy and selection effects with which the real column density distribution in clouds can be mapped. A detailed discussion of this topic can be found in Goodman et al. (2008). The authors conclude that near infrared extinction mapping might provide the 'best' or least biased way to determine the column density distribution of clouds, given a constant gas to dust ratio.

The mapping of extinction at optical and near infrared (NIR) wavelengths can be performed using star counting (e.g. Wolf (1923)), colour excess techniques (e.g. NICE - Lada et al. (1994); NICER - Lombardi & Alves (2001)), or a combination thereof (e.g. Lombardi (2005)). With the availability of large scale homogeneous surveys such as the Digitized Sky Survey (DSS; Lasker (1994)) or the Two Micron All Sky Survey (2MASS; Skrutskie et al. (2006)) the possibility to map the extinction of entire cloud complexes in the Milky Way has arisen. In recent years a number of large scale maps have been created by various authors: Dobashi et al. (2005) (hereafter D05) used optical star counts to map the extinction along the entire Galactic Plane with $|b| < 40^\circ$; Froebrich et al. (2005) used star counts in 2MASS to determine the relative extinction in the entire Galactic Plane with $|b| < 20^\circ$; Large scale maps (e.g. Pipe Nebula, Ophiuchus, Lupus) based on the NICER

⋆ E-mail: jr262@kent.ac.uk,
† E-mail: df@star.kent.ac.uk

Table 1. The different maps created for the project. See text for details.

Number	Description	Type
1	A_V - 25 stars	Con-noise-map
2	A_V - 49 stars	Con-noise-map
3	A_V - 100 stars	Con-noise-map
4	σ_{A_V} - 25 stars	Con-noise-map
5	σ_{A_V} - 49 stars	Con-noise-map
6	σ_{A_V} - 100 stars	Con-noise-map
7	Distance to 25^{th} neighbour	Con-noise-map
8	Distance to 49^{th} neighbour	Con-noise-map
9	Distance to 100^{th} neighbour	Con-noise-map
10	A_V	Con-resolution-map
11	σ_{A_V}	Con-resolution-map

technique are presented e.g. by Lombardi et al. (2006; 2008); A $127^\circ \times 63^\circ$ region towards the Galactic Anticentre region has been mapped by Froebrich et al. (2007) using the NICE technique. Based on far infrared emission maps an all sky extinction map has been created by Schlegel et al. (1998) (hereafter S98).

We plan to study the column density distribution of all clouds in the Milky Way accessible with the NICE technique. As a first step we present here our all sky near infrared extinction maps based on 2MASS. We have created a variety of maps using a fixed grid (constant spatial resolution) method, as well as a nearest neighbour (constant noise) approach. The resulting column density distributions of the clouds will be analysed in a forthcoming publication.

Our paper is organised as follows. In Sect. 2 we describe in detail the method used to determine the extinction maps, including the calibration and the uncertainties. The results are presented in Sect. 3 where we also compare our maps with the existing large scale extinction maps from D05 and S98. A summary is presented in Sect. 4.

2 EXTINCTION MAP DETERMINATION METHOD

2.1 The extinction maps

For the determination of our extinction maps we used the 2MASS Point Source catalogue (Skrutskie et al. (2006)). To ensure that only high photometric quality sources are used, we extracted all objects with the highest quality flag in each of the three filters (Qflag='AAA') from the catalogue. All other sources were disregarded. We extracted positions of all sources from the catalogue, as well as the J, H, and K magnitudes and their associated errors. The coordinates were converted into the Galactic coordinate system using the IRAF[1] task CONVERT.

We have created different maps for the project to facilitate different needs. A summary of all available maps can be found in Table 1. There are two main types of maps: i) Maps that use a fixed number of nearest stars at each position. ii) Maps that use all stars within a fixed area around the position. Effectively the first type of map can be considered as a constant noise - variable spatial resolution map, and the second map as a constant spatial resolution - variable noise map.

i) *Con-noise-maps*: These maps use either the 25, 49, or 100 nearest stars to the central pixel position to determine the *median* J-H, H-K, and J-K colour of stars. The choice of the number of stars basically creates three maps with different spatial resolutions and noise. Thus, the spatial resolution varies by about a factor of 2 between the map using 25 stars and the map using 100 stars. Additionally, we determine maps of the distance to the 25^{th}, 49^{th}, and 100^{th} nearest neighbour (i.e. the spatial resolution at each point). Furthermore a map of the uncertainty in the median colour at each point is created.

ii) *Con-resolution-maps*: For these maps we fixed a radius around the center of each pixel, and all stars closer than that radius were used in the *median* J-H, H-K, and J-K colour determination. As radii we choose 1.7 times the pixel size for an oversampling of about three. We further determined a map of the uncertainties in the median colours.

The pixel size of our maps varies with galactic latitude, according to stellar density. For maps with variable spatial resolution we ensure that the oversampling is on average between 2.5 and 3.5, except in areas of high extinction where larger values are obtained. The pixel size in the maps was varied from $0.5'$ at $b = 0^\circ$ to $2'$ at $|b| = 90^\circ$ with increments of $0.5'$. For the maps with constant resolution the same pixel size as for the *Con-noise-maps* are chosen. With the fixed oversampling this results in a fixed spatial resolution of these maps. The details of how the pixel sizes and spatial resolution depends on $|b|$ are given in Table 2.

Table 2. Pixel sizes and spatial resolution of our maps depending on Galactic Latitude $|b|$. The 'N-A' in the spatial resolution column for the *Con-noise-maps* indicates that the spatial resolution depends on the number of stars (25, 49, or 100) used and also varies with position. A map of the spatial resolution for the map using the nearest 49 stars is shown in the right panel of Fig. 2.

Map type	$\|b\|$ range	Pixel size [$'$]	Spatial resolution [$'$]
Con-noise	90° – 50°	2.0	N-A
	50° – 40°	1.5	N-A
	40° – 20°	1.0	N-A
	20° – 0°	0.5	N-A
Con-resolution	90° – 50°	2.0	6.8
	50° – 40°	1.5	5.1
	40° – 20°	1.0	3.4
	20° – 0°	0.5	1.7

2.2 Extinction determination and calibration

Median colours

We first determine the median colour of all stars at the position of each pixel (depending on the type of map a different number of stars is included in this calculation). For example we prepare a map where each pixel contains the value:

$$[J-H] = Median(m^i_{\rm J} - m^i_{\rm H}) \quad (1)$$

where i runs from 1 to N, with N being the total number of stars included in the calculation at each pixel. $[J-H]$ symbolises the median colour of stars in a pixel (in this case the J-H colour). $m^i_{\rm J}$ and $m^i_{\rm H}$ are the individual 2MASS magnitudes of the stars used for the colour determination.

We use the median colour instead of the mean because of the following: i) It eliminates intrinsically red, young stars, which would systematically influence the mean. This is the case as long as

[1] IRAF is distributed by the National Optical Astronomy Observatories, which are operated by the Association of Universities for Research in Astronomy, Inc., under cooperative agreement with the National Science Foundation.

there are more foreground and background stars than young stars. There are only two obvious cases in our map where the determined colour is dominated by intrinsically red objects and hence not representative of the extinction. These are the areas of the Orion Nebula Cluster and the core of the L 1688 cloud in Ophiuchus (see below). ii) Similarly, clusters of stars with colours different from background and foreground stars are eliminated if they do not dominate the numbers. iii) Most importantly the median ensures that we either measure the correct colour excess/extinction of a cloud or we measure no extinction (i.e. do not detect the cloud at all). As long as there are more background stars to the cloud the median ensures we determine the colour of the background stars, and hence the correct colour excess. If there are more foreground stars to the cloud the median corresponds to the colour of the foreground stars and we do not detect the cloud. For details and a simulation of the recovery of extinction values using this method see Froebrich & del Burgo (2006). This last point is the most important for our work, since we will analyse the column density distribution within the clouds. The use of the mean colour would distort the column density distribution in a non-linear and position/extinction dependent way, which would not allow any of our planned analysis.

Colour excess

Each of our median colour maps has to be converted into the respective colour excess map in order to determine the extinction/column density of material. The median colour of the stars in regions without dust clouds varies with position in the Galaxy due to different stellar populations. We hence need to determine (fit) a function describing the median colour of stars in extinction free regions in the maps. This was done in an iterative way described in the following:

i) The median colour maps were rebinned to a $10'$ per pixel map, and median filtered with a filter size of one degree.

ii) We masked out regions which are influenced by dust clouds. Identification of clouds was initially achieved using the S98 maps and excluding data with E$(B-V) > 0.125$ mag. Once a preliminary A_V map had been produced (see steps iii to v) we repeated this stage but using our extinction map created from $[H-K]$. In this final step we masked out all pixels with $A_V > 0.5$ mag and extended the mask by $40'$ towards unmasked regions to ensure all clouds with significant A_V values are masked out.

iii) We then fit a spline function to the unmasked extinction free regions to establish the colour excess zero point at all positions. At first 1D-spline functions were fit along $10'$ wide columns of constant galactic longitude with knots every degree except in the masked regions. This enabled us to fill in the gaps around the Galactic Plane where no extinction free data is available.

iv) We then fit 1D-spline functions along $10'$ wide rows of constant galactic latitude with knots every degree to the results of step iii). This final background colour array was expanded to the original size and smoothed with a $5'$ radius.

v) We then subtract the result of step iv) from the median colour maps to determine the colour excess, i.e.:

$$\langle J-H \rangle_{(l,b)} = [J-H]_{(l,b)} - fit[J-H]_{(l,b)} \qquad (2)$$

where (l, b) denotes the position in the map.

The colour excess maps are then converted into H-band extinction, assuming a power law for the extinction in the NIR $A_\lambda \propto \lambda^{-\beta}$, with β the near infrared extinction power-law index. The value for β given in the literature varies between 1.6 and 2.0 (see e.g. Martin & Whittet (1990), Drain (2003)). Here we use a value of $\beta = 1.7$. Hence the extinction in the H-band can be determined as:

$$A_{H,\langle J-H \rangle} = \frac{\langle J-H \rangle}{\left(\frac{\lambda_H}{\lambda_J}\right)^{\beta} - 1} \qquad (3)$$

or

$$A_{H,\langle H-K \rangle} = \frac{\langle H-K \rangle}{1 - \left(\frac{\lambda_K}{\lambda_H}\right)^{-\beta}} \qquad (4)$$

Both extinction values can be averaged and converted into optical extinction (A_V) via:

$$A_V = \frac{5.689}{2} \cdot \left(A_{H,\langle J-H \rangle} + A_{H,\langle H-K \rangle}\right) \qquad (5)$$

where the factor 5.689 is the conversion of H-band into optical extinction following Mathis (1990). The (in principle) available third colour excess $\langle J-K \rangle$ is not used, since it is not independent of the two other colours.

Calibration offsets

The extinction maps determined from different colour excess (e.g. $\langle J-H \rangle$ and $\langle H-K \rangle$) should, if we apply the correct extinction law, result in the same extinction values. This also implies that our fit of the median background colour is correct. Near the Galactic Plane and the Galactic Center, however, there are not enough data points/regions that are free of extinction, and hence the fit might not be 100 % accurate. This is in particular a problem close to the Galactic Center, where the population of stars is dominated by giants, compared to away from the Galactic Plane, where normal dwarf stars dominate the stellar population in 2MASS. Thus, the majority of the regions used for the fit of the background colour is dominated by dwarfs. Hence, our fitted function describes the median colours of dwarf stars. In case of the $[H-K]$ colours, there is no severe systematic problem with this, since dwarfs and giants of the same spectral type have basically the same $[H-K]$ colours. Hence, we can assume that our fit in $[H-K]$ is correct everywhere. The situation is very different for $[J-H]$ and $[J-K]$, where giants and dwarfs have different colours. Since we fit these colours using mostly regions dominated by dwarfs, the fit in regions close to the Galactic Center will have systematic offsets. Since giants have redder $[J-H]$ and $[J-K]$ colours than dwarfs of the same spectral type, this will generate a systematic positive offset in the extinction maps created from these colours, compared to the maps generated from $[H-K]$.

We have hence used the extinction maps created from $[H-K]$ as a control and subtracted it from the other maps to check for differences. When determining the difference D_{A_V} between extinction maps obtained from $[J-H]$ and $[H-K]$, we clearly find systematic residuals (see Fig.1). Due to the redder colour of the giants in $[J-H]$ an offset of almost 2 mag in A_V is found in regions close to the Galactic Center. The size scale of these offsets is very large, up to 120° in l. This effect of different colours of giants and dwarfs can also be seen in the Large and Small Magellanic Clouds, which are clearly apparent in the difference map. There are

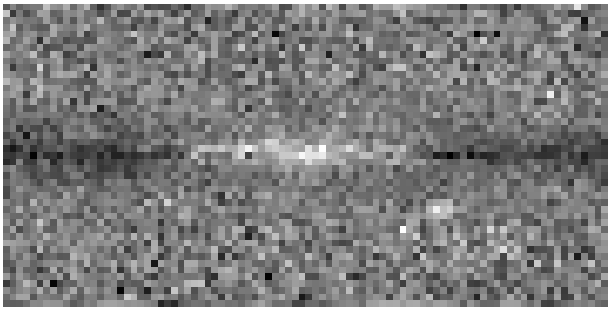

Figure 1. Grey scale representation of the difference map calculated as $D_{A_V} = 5.689 \cdot \left(A_{H,\langle J-H\rangle} - A_{H,\langle H-K\rangle}\right)$ (see text for details). A_V values are scaled linearly from -1.5 mag (black) to +1.5 mag (white). The image size is $360^\circ \times 180^\circ$ with the Galactic Centre in the middle.

also negative offsets near the Galactic Plane. These offsets can be caused by two effects:

i) The region is dominated by young stellar objects with an intrinsic $H-K$ excess due to a disk. While this is the case in the Orion Nebula Cluster and the core of L 1688 in Ophiuchus, it cannot be the cause for the large scale offsets along the entire Galactic Plane.

ii) The region contains a large fraction of higher mass stars (spectral types O-F). Their $[J-H]$ colour is measurably smaller than in the population of low mass dwarfs away from the Galactic Plane used for the fit. Hence, a smaller extinction value is measured. The $[H-K]$ colours are also smaller, but the effect seems to be not as pronounced (i.e. our extinction map calculated from $[H-K]$ does not show negative A_V 'holes' near the Galactic Plane as does the map determined from $[J-H]$).

We thus assume that point ii) is the reason for the large scale negative offsets. There are further small scale variations caused by the effects of variable observing conditions in 2MASS (see below). To correct for all large scale offsets we filtered the difference image D_{A_V} with a filter radius of 4.5° in l and 0.3° in b and subtracted this filtered image from the extinction map created from $[J-H]$. This will calibrate the extinction maps compared to the maps determined from $[H-K]$, and this is also the final map that is used in the determination of the A_V maps presented in this paper (see left panel of Fig. 2 for one example). Note that this assumes that our extinction maps obtained from $[H-K]$ do not show any systematic offsets. Our comparison with the known extinction maps from D05 and S98 in Sect. 3.3 will show that this assumption is valid within the one sigma uncertainties of our map.

2.3 Uncertainties of the extinction maps

Statistical uncertainties

The uncertainties/variances σ_{A_V} of the final extinction maps are calculated via error propagation from 2MASS photometry. The uncertainties of the median colours of stars in each pixel are e.g.:

$$\sigma_{[J-H]} = \frac{1.253}{N} \cdot \sqrt{\sum_{i=1}^{N} (\sigma_J^i)^2 + \sum_{i=1}^{N} (\sigma_H^i)^2} \qquad (6)$$

where N denotes the total number of stars used for this pixel. σ_J^i and σ_H^i are the individual J and H-band uncertainties in the photometry of the star i. The factor 1.253 is caused by the use of the median instead of the mean (Kenney & Keeping (1962)). The uncertainty of the median is larger by this factor than the uncertainty of the mean for large samples and a normal distribution (which we assume for our individual uncertainties).

To determine the uncertainties in the A_V map we assume that the statistical errors of the colour excess values are identical to the variance in the median colour maps. That said, we assume that we only introduce systematic offsets but no additional statistical uncertainties when converting the median colour maps into colour excess maps (see below for details on these systematic offsets). Hence:

$$\sigma_{\langle J-H\rangle} = \sigma_{[J-H]} \qquad (7)$$

The corresponding errors in the H-band extinction determined from the colour excess are then:

$$\sigma_{A_{H,\langle J-H\rangle}} = \frac{\sigma_{\langle J-H\rangle}}{\left(\frac{\lambda_H}{\lambda_J}\right)^{\beta} - 1} \qquad (8)$$

and

$$\sigma_{A_{H,\langle H-K\rangle}} = \frac{\sigma_{\langle H-K\rangle}}{1 - \left(\frac{\lambda_K}{\lambda_H}\right)^{-\beta}} \qquad (9)$$

When determining the variance of the averaged A_V map we have to take into account that the variances of the colours are not independent of each other (see e.g. Froebrich & del Burgo (2006)). We hence need to consider the covariance between the extinction maps determined from $\langle J-H\rangle$ and $\langle H-K\rangle$ colour excess. Hence the variance of the A_V map can be determined by:

$$\sigma^2_{A_V} = \left(\frac{5.689}{2}\right)^2 \cdot \left(\sigma^2_{A_{H,\langle J-H\rangle}} + \sigma^2_{A_{H,\langle H-K\rangle}} + 2 \cdot \sigma_{cov}\right) \qquad (10)$$

where σ_{cov} is the covariance of the two extinction maps. This covariance can in principle be determined in extinction free regions (i.e. no colour excess) in our map. We can calculated it as the average pixel value in the product image of the two H-band extinction maps in areas with no extinction, i.e:

$$\sigma_{cov} = \frac{1}{N} \cdot \sum_{j=0}^{N} \left(\left(A_{H,\langle J-H\rangle}\right)_j \cdot \left(A_{H,\langle H-K\rangle}\right)_j\right) \qquad (11)$$

where j runs over all pixels N in the map with no colour excess. The covariance values found by this way are about $\sigma_{cov} = 0.0015\,\mathrm{mag}^2$. However, the H-band extinction values in our maps are not completely independent from neighbouring pixels, since our spatial resolution is larger than the pixel size. We hence cannot use Eq. 11 to determine σ_{cov}. Instead we determine the covariance in the following way: i) Determine a histogram of extinction values in cloud free regions in our final extinction map. ii) Measure the FWHM or variance σ_{A_V} of the distribution. iii) Using the knowledge of the contribution from $\sigma_{\langle J-H\rangle}$ and $\sigma_{\langle H-K\rangle}$ in Eq. 10 we can determine the covariance.

Using this method we measure typical covariance values from $0.0025\,\mathrm{mag}^2$ to $0.0055\,\mathrm{mag}^2$ in the map for the nearest 49 stars. We use $\sigma_{cov} = 0.004\,\mathrm{mag}^2$ in the final maps. Table 3 lists some individual covariance values for selected areas. Note that this high value for the σ_{cov} means that the covariance dominates the total statistical uncertainties in our maps. We empirically find that the

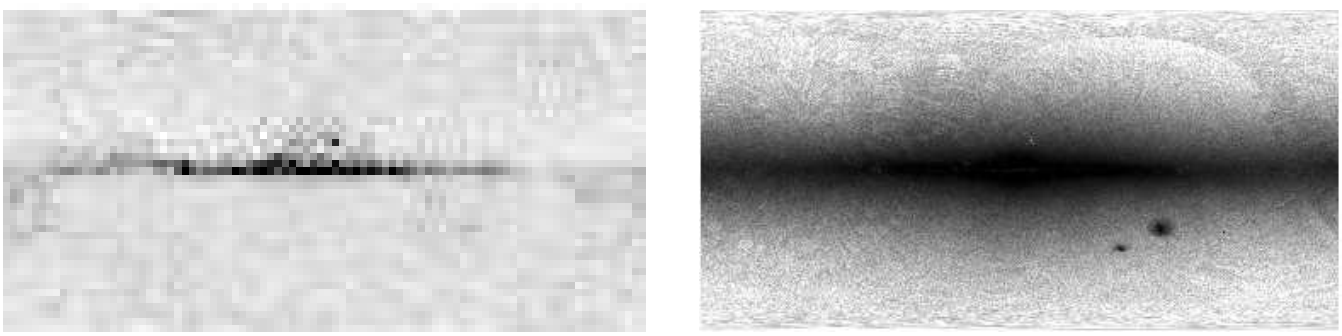

Figure 2. Left Panel: Our all sky extinction map using the nearest 49 stars. The image size is $360^\circ \times 180^\circ$ with the Galactic Centre in the middle. Optical extinction values are scaled linearly from -1 mag (white) to +7 mag (black). **Right Panel:** Grey scale map of the distance to the 49^{th} nearest neighbour, i.e. a spatial resolution map of our data. Grey values are scaled from $1'$ (black) to $11'$ (white). The image scale is the same as in the left panel.

Table 3. Examples of the covariance values σ_{cov} determined in a number of extinction free regions.

l range	b range	σ_{cov} [mag^2]
163.3° – 158.3°	+32.3° – +37.3°	0.0055
31.3° – 26.3°	+31.3° – +36.3°	0.0031
313.3° – 308.3°	+31.9° – +36.9°	0.0026
272.0° – 267.0°	+31.0° – +36.0°	0.0030
143.0° – 138.0°	−35.7° – −30.7°	0.0039
85.1° – 80.1°	−36.0° – −31.0°	0.0037
225.5° – 220.5°	−36.1° – −31.1°	0.0047
244.2° – 239.2°	−37.5° – −32.5°	0.0052

average covariance values for our other constant noise maps can approximately be described by a power-law of the form $\sigma_{cov}(N) \propto N^{-0.8}$, where N denotes the number of stars used to determine the extinction at each pixel. We use this equation to determine the covariance values for the constant resolution map, because this map uses a different number of stars at each pixel and our σ_{cov} determination method described above cannot be applied.

Figure 3 shows the distribution of the individual statistical uncertainties for all pixels in a 25 square degree region near the Galactic Plane ($2.5^\circ < b < 7.5^\circ$; $221.67^\circ < l < 226.67^\circ$) for all of our maps. In Table 4 we list the peak position of the σ_{A_V} distribution for a sample of areas in our map using the nearest 49 stars.

Systematic uncertainties

So far we have only considered the statistical uncertainties in our maps. The fitting of the background median colours to obtain the colour excess values, as well as potential changes in the extinction law, will add further uncertainties to our σ_{A_V} estimate. The variances due to these points should in principle be added into Eq. 10. Since all these uncertainties are systematic in nature and on different scales, we do not add them into the uncertainty maps presented here, but will discuss the scale and magnitude of the terms in the following.

i) The fit of the background colours will introduce systematic offsets into the extinction maps if it is not perfect. The angular scale of these offsets will, however, be large, due to the nature of the fitted function. Hence the scale of any systematic offsets will be much larger than 4.5° in l and 0.3° in b, the smallest filter size used in the process of calibration. These offsets will hence not influence any analysis of the column density distributions of molecular clouds in the maps, in particular away (more than 1°) from the Galactic Plane. They will only lead to small offsets in the absolute A_V values. The magnitude of these offsets can be estimated from the systematic comparison of our map with the maps of D05 and S98. We find in Sect. 3.3, that the offsets are generally not larger than the one sigma variance of the extinction.

ii) There are small scale (typically $\sim 14'$ by $\sim 6'$) systematic offsets caused by the 2MASS observing procedure. Different observing conditions have lead to varying completeness limits in the 2MASS data. The different completeness limits cause the median colours of the stars to change locally in the catalogue. For example at better conditions more fainter stars are detected and these are usually redder. This is particularly obvious in $[H-K]$, since deeper observations generally pick up more nearby dwarf stars, which tend to be redder in $[H-K]$, but will not influence the $[J-H]$ colour. We do not cap the stars included in the determination of our map at a global completeness limit, however, since this would reject too many objects and seriously degrade the achievable spatial resolution in many parts of the map. The magnitudes of the extinction offsets are up to 1 mag A_V in the maps determined from $[H-K]$, and only up to 0.5 mag A_V in the maps determined from $[J-H]$. Hence, the maps determined from median $[J-H]$ colours suffer much less and should be used if a locally absolutely calibrated A_V map is required. Note that in our final averaged A_V maps these small scale variations can be as large as two times the statistical variance. Hence, care needs to be taken when analysing the column density distribution in these maps. In particular, any cloud structures aligned with the 2MASS observing pattern should be considered carefully.

iii) A spatially variable extinction law could introduce offsets that are non-systematic and small scale. A change of the extinction law from the interstellar value might be expected in higher column density regions, where coagulation of dust grains and/or the formation of ice mantels might change the optical properties (e.g. Ossenkopf (1993), Preibisch et al. (1993), Larson & Whittet (2005)). If the β value of the extinction law changes by ± 0.2 compared to our applied value of 1.7, a change in optical extinction of about 10 % will be the result. Given our average statistical uncertainties of about 0.28 mag for the map using the nearest 49 stars (see Table 4), possible variations in the extinction law will only lead to measurable effects at A_V values larger than 8 mag (three sigma detections). The applied constant value of $\beta = 1.7$ is hence justified. Furthermore, there is no residual cloud structure visible in the D_{A_V} map (Fig. 1), emphasising that in general the assumption of a constant β value is valid. We will investigate possible small scale variations of β in a forthcoming paper.

Table 4. Summary table of the properties of selected regions in our map. We list the region name, the area, the peak in the distribution of uncertainties in the map using the nearest 49 stars, the slope and offsets of the extinction when compared between our map, D05 and S98. The (*) indicates slopes and offsets that have been fit by eye, since no satisfactory linear regression fit could be achieved.

Region	Name	l range	b range	σ_{A_V}	D05 vs Our map		S98 vs Our map		S98 vs D05	
				[mag]	offset	slope	offset	slope	offset	slope
1	Camelopardalis	157.2° - 152.2°	1.4° - 6.4°	0.286	0.22	1.21	-0.52	0.52	-0.61	0.36
2	Serpens	31.3° - 26.3°	1.3° - 6.3°	0.282	0.17	1.28	-1.70*	1.00*	-1.40*	0.80*
3	Lupus	341.8° - 336.8°	1.9° - 6.9°	0.282	0.82	1.06	-0.34	0.73	-0.80*	0.60*
4	Vela	272.0° - 267.0°	1.0° - 6.0°	0.281	0.22	1.41	-0.86	0.70	-0.48	0.37
5	Taurus	166.0° - 161.0°	4.9° - 9.9°	0.282	0.19	1.13	-0.31	0.62	-0.54	0.56
6	North America Nebula	85.0° - 80.0°	1.0° - 6.0°	0.278	0.19	1.34	-0.74	0.73	-0.42	0.46
7	Monoceros	225.5° - 223.5°	1.0° - 6.0°	0.281	-0.01	1.23	-0.48	0.58	-0.70*	0.55*
8	Auriga	185.0° - 180.0°	3.0° - 8.0°	0.281	0.11	1.23	-0.58	0.65	-0.63	0.46

2.4 Other Methods

There are, of course, other methods available to determine extinction maps based on NIR photometry. These are in particular the NICER method presented by Lombardi & Alves (2001), or the work presented by Lombardi (2005). These methods are based on the minimisation of the variance of the determined A_V values by optimally combining the available colour and position information. Naturally, these methods will have a smaller variance than our method. The reduction in noise when using the NICER method with respect to the simpler averaging of colour excess values applied by us is typically of the order of about 20 % (see e.g. Froebrich et al. (2007)). This would e.g. lower the $3\,\sigma$ detection limit in our standard map from 0.84 mag to 0.70 mag. However, possible variations/uncertainties in the applied extinction law, as well as small scale changes in the completeness limit (see Sect. 2.3) result in similar size variations of the A_V values. Furthermore, this small gain in signal-to-noise has to be weighted against the immense additional computational costs of the more sophisticated methods. These computational costs, as well as the simplicity and robustness of the colour excess technique are hence the essential arguments for our choice of technique.

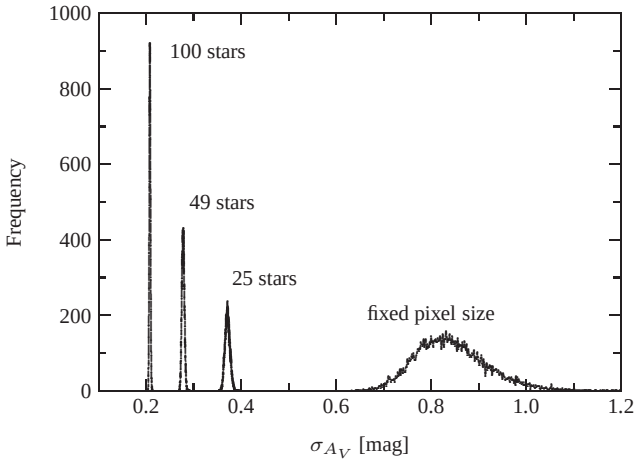

Figure 3. Distribution of the individual statistical uncertainties of our A_V values in a 25 square degree region near the Galactic Plane ($2.5° < b < 7.5°$; $221.67° < l < 226.67°$). We show the one sigma variance distribution σ_{A_V} for the maps using the nearest 25 (peak at about 0.21 mag), 49 (peak at about 0.28 mag), 100 stars (peak at about 0.37 mag), and the constant pixel size map (peak at about 0.83 mag). Note that the peaks of the distributions will not change with position for the *con-noise* maps (see e.g. Table 4) since the same number of stars is included in the A_V calculation. The spatial resolution of the 49^{th} nearest neighbour map in the area for which the histograms are plotted is about a factor of three higher compared to the fixed pixel size map, hence the larger noise in the latter.

3 RESULTS

3.1 A_V and spatial resolution maps

We have created a number of all sky near infrared extinction maps for our project. The available maps are listed in Table 1. They will all be made available on the CDS and can also be downloaded at `http://astro.kent.ac.uk/extinction`.

In the left panel of Fig. 2 we show a grey scale representation of our all sky A_V map using the nearest 49 stars. Extinction values are scaled linearly between -1 mag (white) and +7 mag (black) of optical extinction. The general distribution of dust along the plane of the Galaxy is immediately visible, as well as the more nearby higher latitude clouds such as Orion, Ophiuchus, Chameleon, Taurus, etc.. The lack of any significant dust away from the Galactic plane is also clear. Features such as the Large and Small Magellanic Clouds can also be seen, and are caused by their red giants (see the discussion above about the calibration of the maps). Some low A_V regions are noticeable in the southern half of the image, at latitudes of $b \approx$-70°. The $E(B-V)$ map of S98 shows material in these positions as well, indicating that the clouds are real. In Appendix B we show detailed high resolution cut-outs of the entire 49^{th} nearest neighbour map for clarity. There we present $32° \times 41°$ sized images. For better contrast the extinction values are scaled by square root from 0 mag to 15 mag optical extinction.

The map of the distance to the 49^{th} nearest neighbour star is shown in the right panel of Fig. 2. It varies from about $1'$ at $b \approx 0°$ to $10'$ at $|b| \approx 90°$. This clearly shows that the spatial resolution varies by about a factor of 10 from near the Galactic Plane to the poles in the image. The map further shows that the spatial resolution is better than $3'$ to $5'$ in all regions of interest, i.e. regions that contain giant molecular clouds, and generally better than $10'$ for $|b| < 30°$.

3.2 Distribution of uncertainties

Most of our maps use a fixed number of stars around the pixel position to determine the extinction. Since most of the selected stars have very similar photometric uncertainties, we named those maps *constant noise maps*. On the other hand, the map using a fixed pixel

size will use a different number of stars and hence result in a more variable noise.

In Fig. 3 we plot the distribution of the one sigma variance in our map for a 25 square degree region near the Galactic Plane ($2.5^\circ < b < 7.5^\circ$; $221.67^\circ < l < 226.67^\circ$). For the constant noise maps the peaks in the distributions are very narrow (justifying the name), while for the constant resolution map the uncertainties vary by a much larger amount even in this rather small field of view. The main cause is that the covariance dominates the variance in the maps, as seen in Sect. 2.3. There are some pixels in the constant resolution map where the noise and the extinction cannot be determined since no stars are found in these pixels. Note that the spatial resolution of the 49^{th} nearest neighbour map in the area for which the histograms are plotted is about a factor of three larger compared to the fixed pixel size map, which explains the larger values of the uncertainties in the latter.

For the constant noise maps the peaks in the variance distribution are at 0.21 mag, 0.28 mag, and 0.37 mag for the 25^{th}, 49^{th}, and 100^{th} nearest neighbour map respectively. This means, that e.g. in the 49^{th} nearest neighbour map, the important threshold for self-shielding of molecular clouds of 1 mag A_V (Hartmann et al. (2001)) is detected always with a signal-to-noise ratio of larger than three.

3.3 Comparison with other large scale extinction maps

To validate our calibration and to compare our new map with existing works we facilitate the widely used all sky extinction map from S98 and the $|b| \leq 40^\circ$ map from D05.

D05 produced A_V maps at angular resolutions of $6'$ and $18'$, covering the sky in the galactic latitude range $|b| \leq 40^\circ$. They performed star counts in the optical data from the Digitized Sky Survey (Lasker (1994)). The wavelengths used lead to a better tracing of low extinction regions in their maps, but underestimate A_V in areas of high extinction.

S98 produced an all sky map of $E(B-V)$, intended for use as a new estimator of Galactic extinction. They used data from COBE/DIRBE and IRAS/ISSA maps. The diffuse emission from dust in the infrared can be used as a measure of column density once the temperature and emissivity is known. The resolution of the final $E(B-V)$ map of S98 is $6.1'$.

Visual Comparison

In Fig. 4 we compare a section of our A_V map (left panel) with the maps of D05 (middle) and S98 (right). Extinction values are scaled linearly between 0.5 and 20 mag. The maps show a region ($20^\circ < l < 30^\circ$ and $0^\circ < b < 10^\circ$) containing the Serpens molecular cloud complex, that nicely illustrates the differences between the maps.

The most obvious difference is the higher spatial resolution of our map (between $2'$ and $4'$) compared to the other two maps (about $6'$). Hence, much finer details, such as small, high column density cores and small scale structures are visible only in our new map.

When comparing our map with D05 there are two further main differences: i) There is a number of very high A_V regions not detected in the D05 map (e.g. the main Serpens core). The reason is that optical star counts are not able to trace such high column densities. ii) Near the Galactic Plane (positioned along the bottom of the image) all but a few clouds are undetected in D05. Again the reason is the rather low penetration depth of the optical star counting technique. The near infrared colour excess method applied by us is able to trace much higher column density regions. However, high A_V regions very close to the plane are also not picked up by our technique. These are regions where foreground stars dominate the stellar population and our median colour excess approach breaks down. Such regions are apparent as 'white' low extinction regions near the bottom in the left panel of Fig. 4.

A comparison of our map with S98 also shows two main differences: i) On average the A_V values from S98 are about a factor of 1.5 to 2 higher. This has already been commented on by D05, and is probably caused by systematic uncertainties in the assumed dust temperature and emissivity in S98. ii) There are very high extinction regions in the densest cores and within 1° of the Galactic Plane visible only in S98. The isolated high extinction cores are probably superimposed point sources and/or regions with significantly different dust temperatures. The high A_V region near the plane is partly caused by the same effect. Additionally the far infrared map basically traces the entire emission from the galactic disk, while our technique has a limit of about 5-8 kpc (e.g. Marshall et al. (2006), Froebrich & del Burgo (2006)).

Detailed comparison with Dobashi et al. (2005)

A more detailed comparison of our map with the D05 maps is shown in Fig. 5, were we plot the D05 A_V values against ours. The figure contains data points from the $5^\circ \times 5^\circ$ region 2 (Serpens), whose coordinates are listed in Table 4. Note that we only plot a random selection of less than 1 % of the data points from the entire area, to facilitate visibility. A one-to-one line, as well as a linear fit (excluding outliers) to the data points are overplotted. The parameters of the linear fit are listed in Table 4 for all regions. The individual comparison plots for all other regions listed in Table 4 are shown in Appendix A1.

We see in Fig. 5 that D05 systematically underestimates the extinction by about 20 % compared to our values. There is on the other hand no systematic offset, i.e. the linear fit has an offset of 0.17 mag, well below the one sigma variance of our A_V values. At high column densities (above 5-6 mag A_V) there are very large differences between the two methods. These are caused by two effects: i) As mentioned earlier, the optical star counting method of D05 is not able to trace these very high extinction regions; ii) Our better spatial resolution allows us to pick up more small scale, high column density cores.

In general the plots for all regions (Appendix A1) show a similar behaviour, i.e. a slight systematic underestimate of A_V in D05 compared to our map and an offset below the variance of our data (see Table 4 for the linear fit parameters). The fact that the offsets are below the variance level in our map, shows that our calibration of the colour excess values has worked properly at all positions. The only region tested where the offset is above the one sigma variance is Lupus. An inspection of the actual plot (Fig. A3), however, shows that a linear fit to the data is certainly not appropriate in this region. The large number of small scale high A_V cores in the field (see also Lombardi et al. (2008)) might cause the very different appearance of the plot.

With a few exceptions, the slope of the linear fits is about 1.2 (see Table 4). There are two possible explanations for this: i) We have used an incorrect extinction law; ii) There are systematic uncertainties in the star count technique;

There are two reasons why explanation i) is unlikely to be the dominant cause for the discrepancy. Firstly, we do not find any residuals resembling the giant molecular clouds when comparing the H-band extinction maps determined from $\langle J-H \rangle$ and

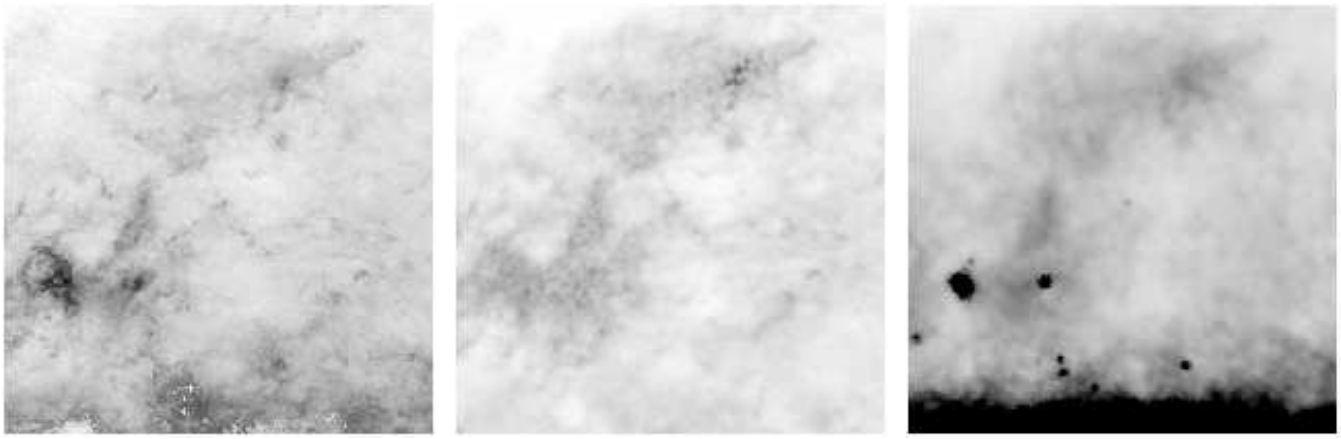

Figure 4. Grey scale representation of region 2 (Serpens) of our A_V map (left panel), the map of D05 (middle panel), and the map of S98 (right panel). The images are $10^\circ \times 10^\circ$ in size and encompass a coordinate range of $20^\circ < l < 30^\circ$ and $0^\circ < b < 10^\circ$. The extinction values in all maps are scaled linearly. White represents 0.5 mag optical extinction, while black represents 20 mag A_V.

$\langle H-K \rangle$ colour excess (see Fig. 1). Such systematic differences should occur if we had used an incorrect extinction law. Secondly, to explain the 20 % difference, a value in excess of $\beta = 2.2$ has to be used in the conversion of colour excess into extinction for all clouds. Even if such values can be found in some clouds, generally a value of $\beta < 2.0$ is found (e.g. Martin & Whittet (1990), Drain (2003)).

Explanation ii) seems to describe a more plausible cause for the 20 % difference. The star counting technique from D05 counts the number of stars in a certain area. With an increasing distance of the cloud an increasing fraction of the stars are foreground. Thus, the further away the cloud is, the more the extinction is underestimated by star counting. Our *median* colour excess method on the other hand will either detect the correct colour excess of stars behind the cloud, or not detect the cloud at all (see above). Simulations of both extinction determination methods in Froebrich & del Burgo (2006) show this effect (their Fig. 9), and that its magnitude is in the order of 20 %. We expect that with an increasing cloud distance the difference between our A_V values and D05 increases. There is a tentative hint of that in the regions selected in Table 4, but we will analyse this in more detail in a forthcoming paper.

Detailed comparison with Schlegel et al. (1998)

We also compare our A_V values to those obtained in S98 for the same set of regions as above. As an example we show the comparison for region2 (Serpens) in Fig. 6. All other individual plots are presented in Appendix A2. The parameters of the linear fits are also given in Table 4.

For the Serpens region there seems to be a general offset of about 1.7 mag A_V between S98 and our map. There are, however, notable exceptions where either the S98 or our map indicates much larger extinction values. The causes for these are either our higher spatial resolution (our A_V higher than S98) or possibly groups of point sources not removed in the S98 maps (in particular near the Galactic Plane) in combination with the limitations of our method to pick up very high column density regions (S98 A_V values higher than ours). In general, we find that the S98 values overestimate the extinction by a factor of about 1.5 to 2.0. This in in agreement with D05, who found an overestimate of A_V from S98 compared with their data by up to a factor of two. The offsets between the two extinction values are generally higher than our one sigma variance. The main reason for these differences are uncertainties in the dust temperature and emissivity, as well as the much larger line of sight in the S98 data. For details we refer to the discussion in D05.

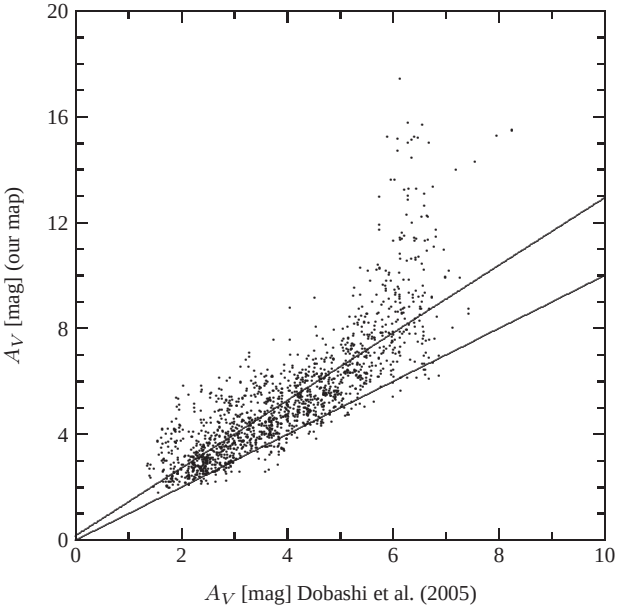

Figure 5. Comparison of the optical extinction values for the region Serpens between our extinction map and the map from D05. As a solid line we overplot a one-to-one line, as well as a linear fit. See Table 4 for the parameters of the fit.

For completeness reasons we have also plotted the A_V values of S98 against D05 in Fig. A3. The results of the linear fits are also listed in Table 4.

4 SUMMARY AND CONCLUSIONS

We have determined a number of all sky near infrared extinction maps using the 2MASS point source catalogue. Constant spatial resolution maps (and hence variable noise) as well as constant noise maps (and hence variable spatial resolution) using either the nearest

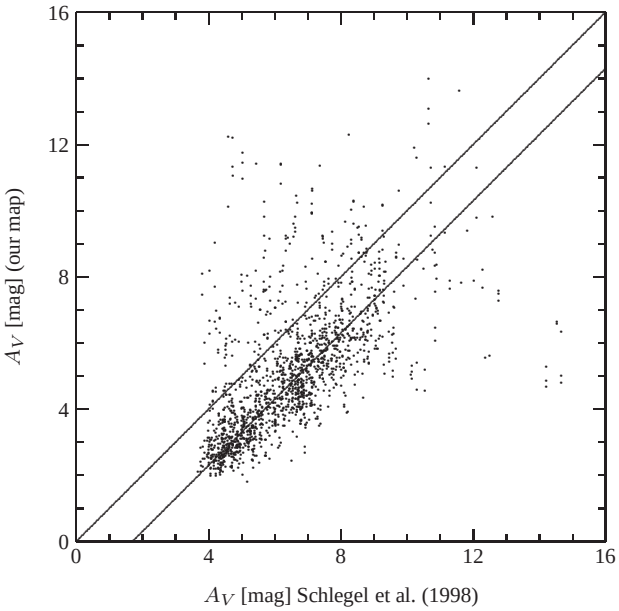

Figure 6. Comparison of the optical extinction values for the region Serpens between our extinction map and the map from S98. As solid line we overplot a one-to-one line, as well as a linear fit. See Table 4 for the parameters of the fit.

25, 49, or 100 stars are presented. We apply a *median* colour excess technique to accurately determine the column density distribution of all nearby giant molecular clouds. Median colours are converted into colour excess by means of a spline fit to extinction free regions.

Our *standard* A_V map uses the nearest 49 stars around each position for the extinction determination. The distance to the 49^{th} nearest star varies between $1'$ near the Galactic Plane to about $10'$ at the poles. The one sigma variance in the map is 0.28 mag A_V. This means that all regions with an optical extinction of more than one magnitude (the important threshold for self-shielding of molecular clouds - Hartmann et al. (2001)) are detected with a signal-to-noise ratio above 3.6.

A comparison with the existing large scale extinction maps from Dobashi et al. and Schlegel et al. has been performed. This comparison shows that our calibration of the A_V values is accurate in the entire map to within the one sigma variance on scales of a few degrees. It further reveals systematic differences in the extinction values compared to Dobashi et al. (our values are $\sim$20 % larger) and Schlegel et al. (our values are $\sim$40 % smaller). This can be attributed to the star counting technique (D05) and systematic uncertainties in the dust temperature and emissivity (S98).

All our extinction maps have been determined in a uniform way for the entire sky. The variety of different spatial resolutions and hence signal-to-noise ratios provides an excellent homogeneous set of extinction values for different needs. Our applied technique does not suffer from systematic uncertainties in the dust temperature and emissivity, or from distance dependent offsets. The spatial resolution is comparable or superior to other existing all sky A_V maps for $|b| < 30^\circ$. Only in some regions with $|b| < 1^\circ$ does our map suffer from a non-detection of clouds due to the domination of foreground stars and different methods such as the usage of longer wavelength data should be applied (e.g. Schultheis et al. (2008)).

ACKNOWLEDGEMENTS

JR acknowledges a University of Kent scholarship. This publication makes use of data products from the Two Micron All Sky Survey, which is a joint project of the University of Massachusetts and the Infrared Processing and Analysis Center/California Institute of Technology, funded by the National Aeronautics and Space Administration and the National Science Foundation.

REFERENCES

Dobashi, K., Uehara, H., Kandori, R., Sakurai, T., Kaiden, M., Umemoto, T., Sato, F., 2005, PASJ, 57, 1
Draine, B.T., 2003, ARA&A, 41, 241-289
Froebrich, D. & del Burgo, C. 2006, MNRAS, 369, 1901
Froebrich, D., Murphy, G.C., Smith, M.D., Walsh, J., Del Burgo, C., 2007, MNRAS, 378, 1447-1460
Froebrich, D., Ray, T.P., Murphy, G.C., Scholz, A., 2005, A&A, 432, L67-L70
Goodman, A.A., Pineda, J.E., Schnee, S.L., 2008, 0806.3441
Hartmann, L., Ballesteros-Paredes, J. & Bergin, E.A. 2001, ApJ, 562, 852
Kenney, J.F. Keeping, E.S., 1962, in Mathematics of Statistics, Pt. 1, 3rd ed. Princeton, NJ: Van Nostrand, p. 211
Lada, C.J., Lada, E.A., 2003, ARA&A, 41, 57
Lada, C.J., Lada, E.A., Clemens, D.P., Bally, J., 1994, ApJ, 429, 694-709
Larson, K.A., Whittet, D.C.B. 2005, ApJ, 623, 897
Lasker, B. M., 1994, in Bulletin of the American Astronomical Society, 26, 914
Lombardi, M., 2005, A&A, 438, 169-185
Lombardi, M., Alves, J., 2001, A&A, 377, 1023-1034
Lombardi, M., Alves, J., Lada, C.J., 2006, A&A, 454, 781-796
Lombardi, M., Lada, C.J., Alves, J., 2008, A&A, 489, 143-156
Marshall, D.J., Robin, A.C., Reylé, C., Schultheis, M., Picaud, S. 2006, A&A, 453, 635
Martin, P.G., Whittet, D.C.B., 1990, ApJ, 357, 113-124
Mathis, J.S., 1990, ARA&A, 28, 37-70
Ossenkopf, V., 1993, A&A, 280, 617-646
Passot, T., Vázquez-Semadeni, E., 1998, PhRvE, 58, 4501
Preibisch, T., Ossenkopf, V., Yorke, H.W., Henning, T., 1993, A&A, 279, 577-588
Schlegel, D.J., Finkbeiner, D.P., Davis, M., 1998, ApJ, 500, 525
Schultheis, M., Sellgren, K., Ramirez, S., Stolovy, S., Ganesh, S., Glass, I. S., Girardi, L. 2008, å, in press
Skrutskie, M.F., Cutri, R.M., Stiening, R., Weinberg, M.D., Schneider, S., Carpenter, J.M., Beichman, C., and et al., 2006, AJ, 131, 1163-1183
Vázquez-Semadeni, E., García, N., 2001, ApJ, 557, 727
Wolf, M., 1923, Astronomische Nachrichten, 219, 109

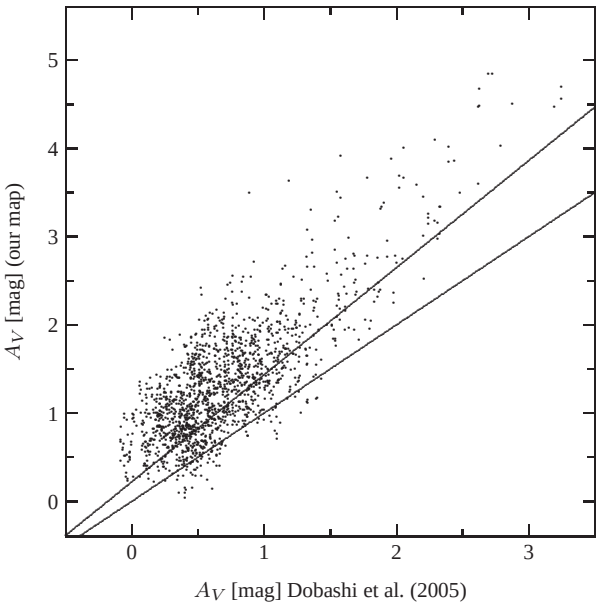

Figure A1. Comparison of the optical extinction values for region1 (Camelopardalis) in Table 4 between our extinction map and the map from D05. As solid line we overplot a one-to-one line, as well as a linear fit. See Table 4 for the parameters of the fit.

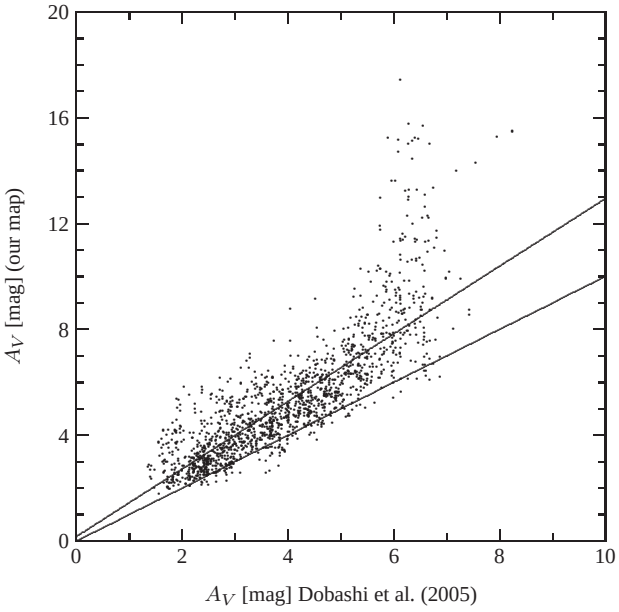

Figure A2. Comparison of the optical extinction values for region2 (Serpens) in Table 4 between our extinction map and the map from D05. As solid line we overplot a one-to-one line, as well as a linear fit. See Table 4 for the parameters of the fit.

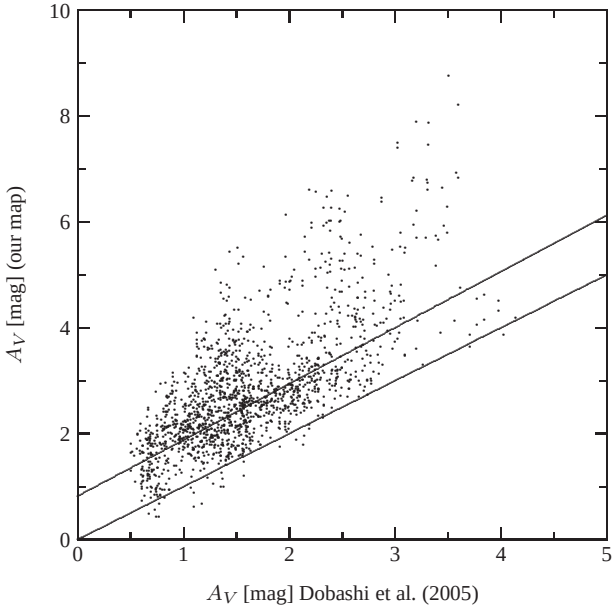

Figure A3. Comparison of the optical extinction values for region3 (Lupus) in Table 4 between our extinction map and the map from D05. As solid line we overplot a one-to-one line, as well as a linear fit. See Table 4 for the parameters of the fit.

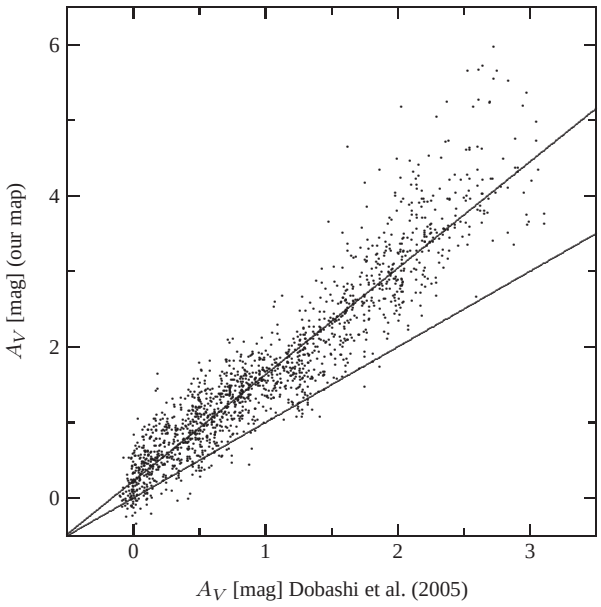

Figure A4. Comparison of the optical extinction values for region4 (Vela) in Table 4 between our extinction map and the map from D05. As solid line we overplot a one-to-one line, as well as a linear fit. See Table 4 for the parameters of the fit.

APPENDIX A: COMPARISON OF MAPS FOR DIFFERENT REGIONS

A1 Our Map vs. Dobashi et al. (2005)

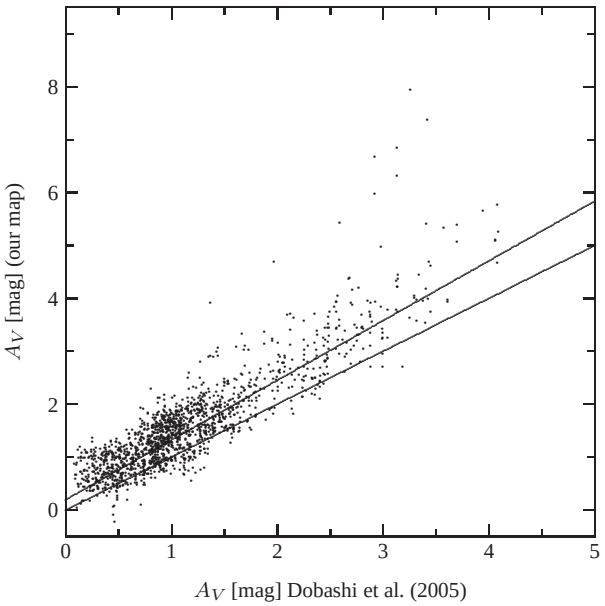

Figure A5. Comparison of the optical extinction values for region5 (Taurus) in Table 4 between our extinction map and the map from D05. As solid line we overplot a one-to-one line, as well as a linear fit. See Table 4 for the parameters of the fit.

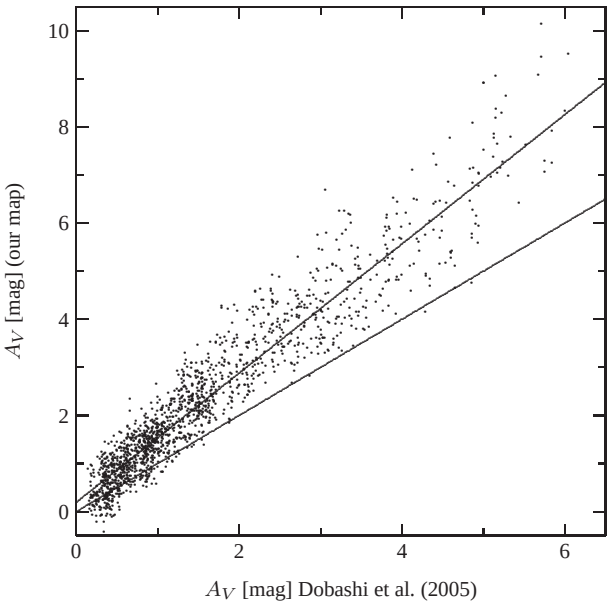

Figure A6. Comparison of the optical extinction values for region6 (North America Nebula) in Table 4 between our extinction map and the map from D05. As solid line we overplot a one-to-one line, as well as a linear fit. See Table 4 for the parameters of the fit.

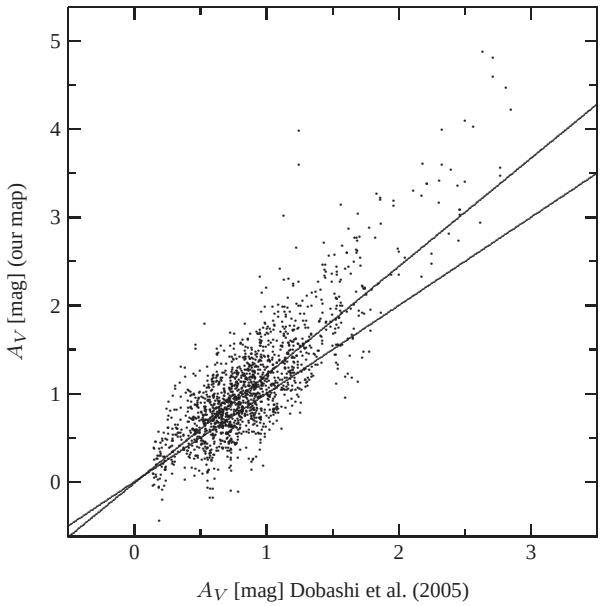

Figure A7. Comparison of the optical extinction values for region7 (Monoceros) in Table 4 between our extinction map and the map from D05. As solid line we overplot a one-to-one line, as well as a linear fit. See Table 4 for the parameters of the fit.

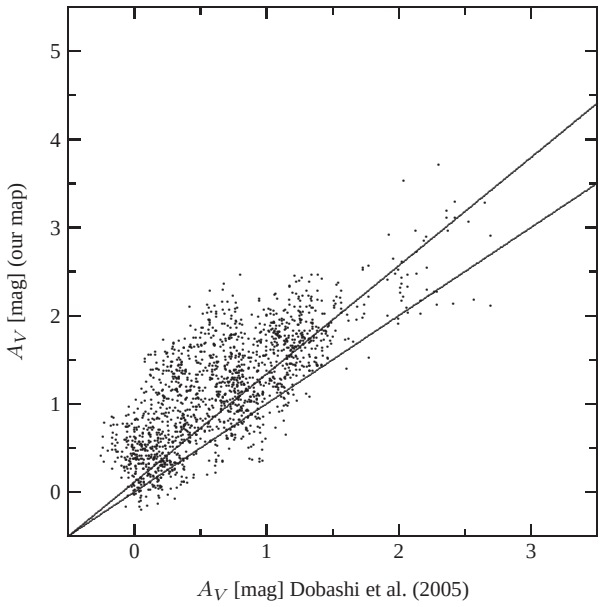

Figure A8. Comparison of the optical extinction values for region8 (Auriga) in Table 4 between our extinction map and the map from D05. As solid line we overplot a one-to-one line, as well as a linear fit. See Table 4 for the parameters of the fit.

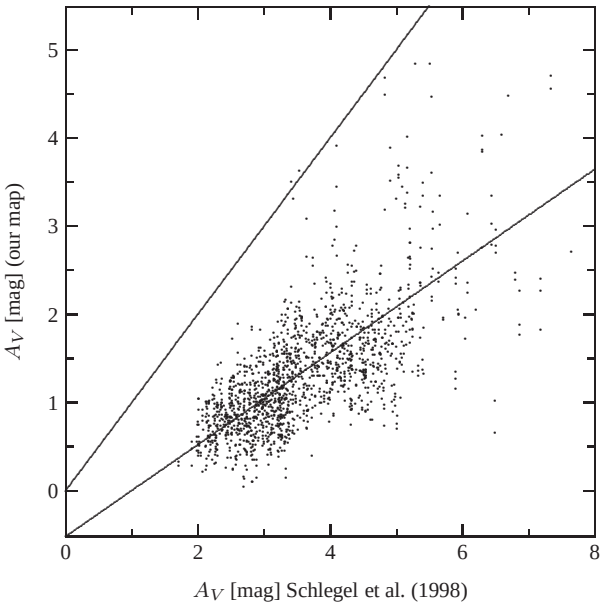

Figure A9. Comparison of the optical extinction values for region1 (Camelopardalis) in Table 4 between our extinction map and the map from S98. As solid line we overplot a one-to-one line, as well as a linear fit. See Table 4 for the parameters of the fit.

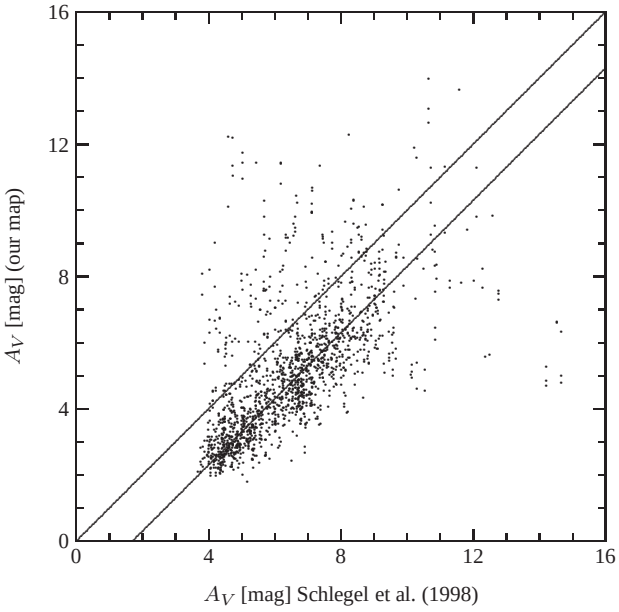

Figure A10. Comparison of the optical extinction values for region2 (Serpens) in Table 4 between our extinction map and the map from S98. As solid line we overplot a one-to-one line, as well as a linear fit. See Table 4 for the parameters of the fit.

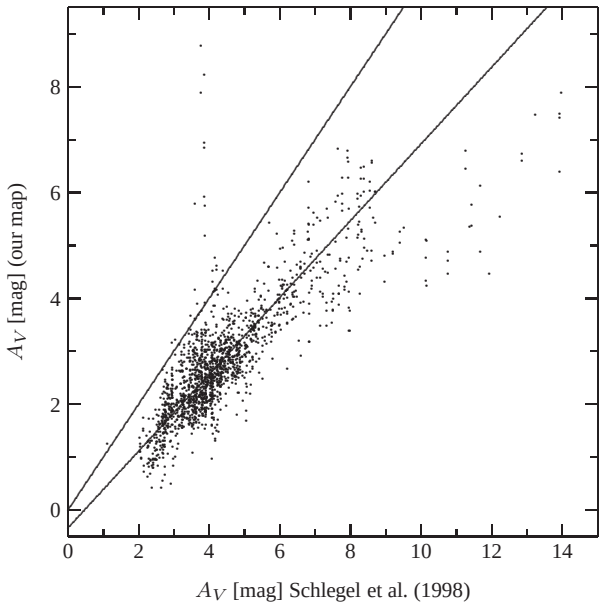

Figure A11. Comparison of the optical extinction values for region3 (Lupus) in Table 4 between our extinction map and the map from S98. As solid line we overplot a one-to-one line, as well as a linear fit. See Table 4 for the parameters of the fit.

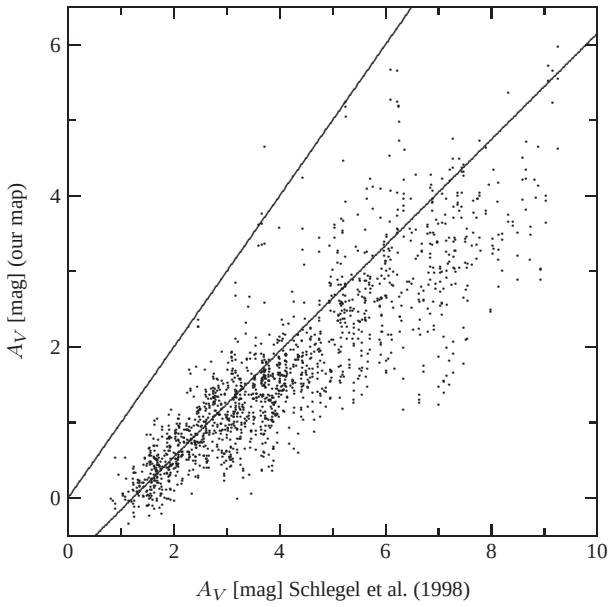

Figure A12. Comparison of the optical extinction values for region4 (Vela) in Table 4 between our extinction map and the map from S98. As solid line we overplot a one-to-one line, as well as a linear fit. See Table 4 for the parameters of the fit.

A2 Our Map vs. Schlegel et al. (1998)

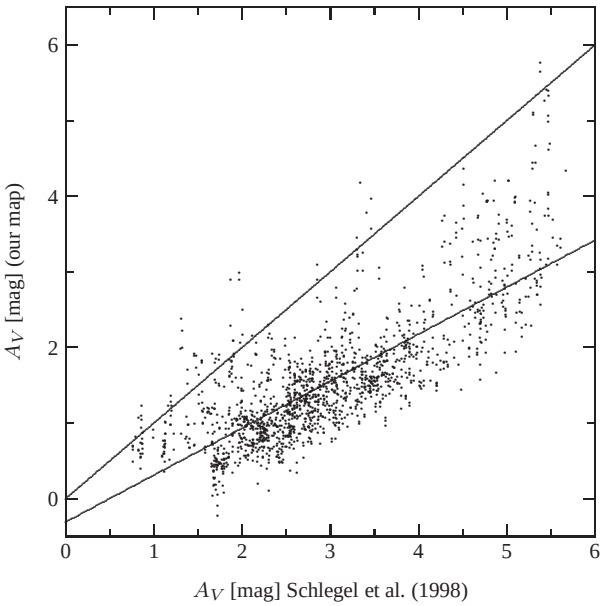

Figure A13. Comparison of the optical extinction values for region5 (Taurus) in Table 4 between our extinction map and the map from S98. As solid line we overplot a one-to-one line, as well as a linear fit. See Table 4 for the parameters of the fit.

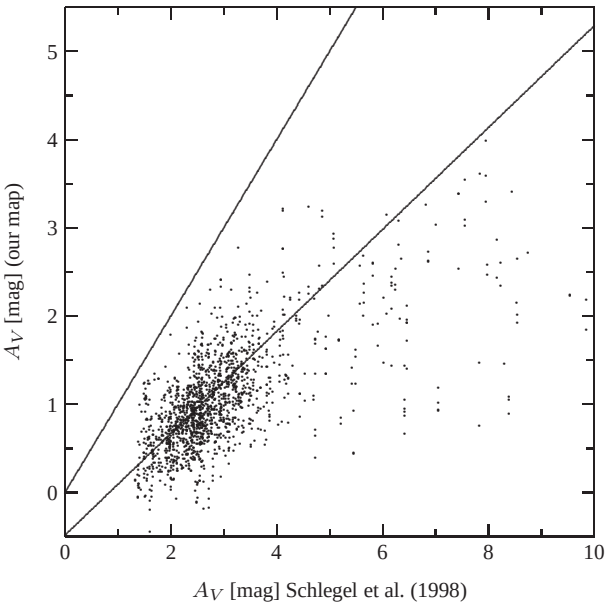

Figure A15. Comparison of the optical extinction values for region7 (Monoceros) in Table 4 between our extinction map and the map from S98. As solid line we overplot a one-to-one line, as well as a linear fit. See Table 4 for the parameters of the fit.

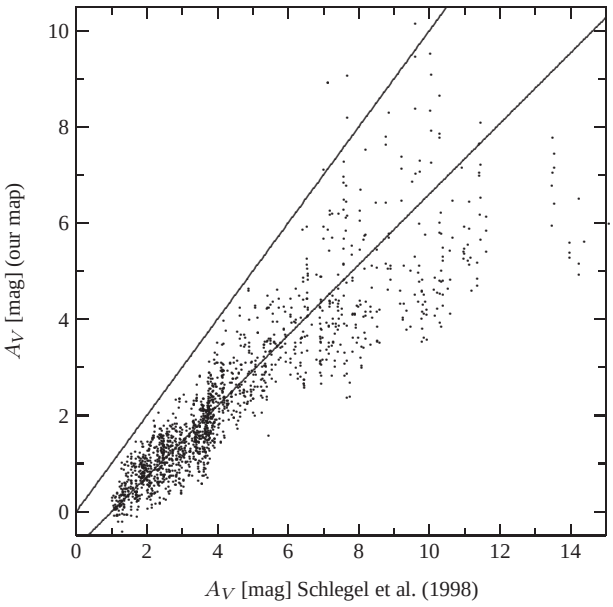

Figure A14. Comparison of the optical extinction values for region6 (North America Nebula) in Table 4 between our extinction map and the map from S98. As solid line we overplot a one-to-one line, as well as a linear fit. See Table 4 for the parameters of the fit.

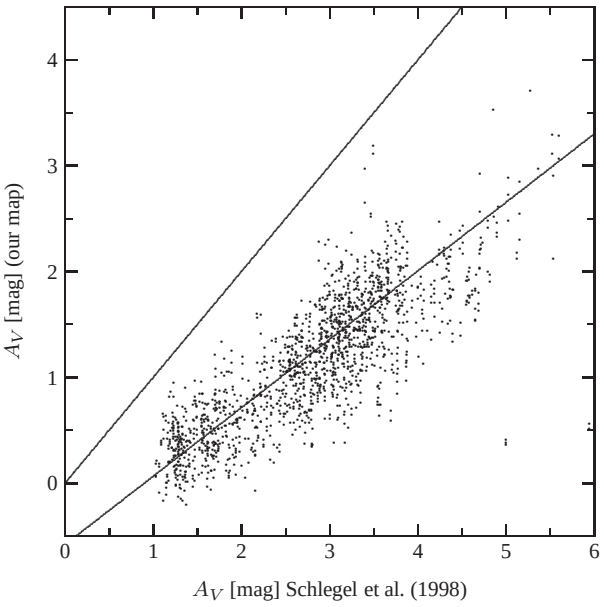

Figure A16. Comparison of the optical extinction values for region8 (Auriga) in Table 4 between our extinction map and the map from S98. As solid line we overplot a one-to-one line, as well as a linear fit. See Table 4 for the parameters of the fit.

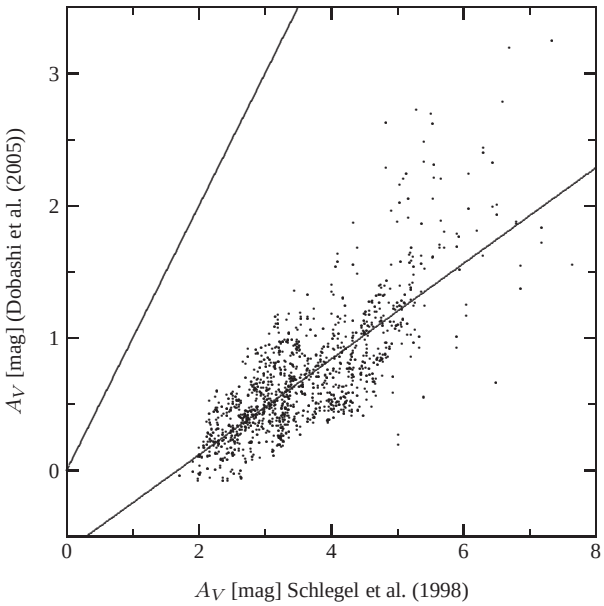

Figure A17. Comparison of the optical extinction values for region1 (Camelopardalis) in Table 4 between the map of D05 and the map from S98. As solid line we overplot a one-to-one line, as well as a linear fit. See Table 4 for the parameters of the fit.

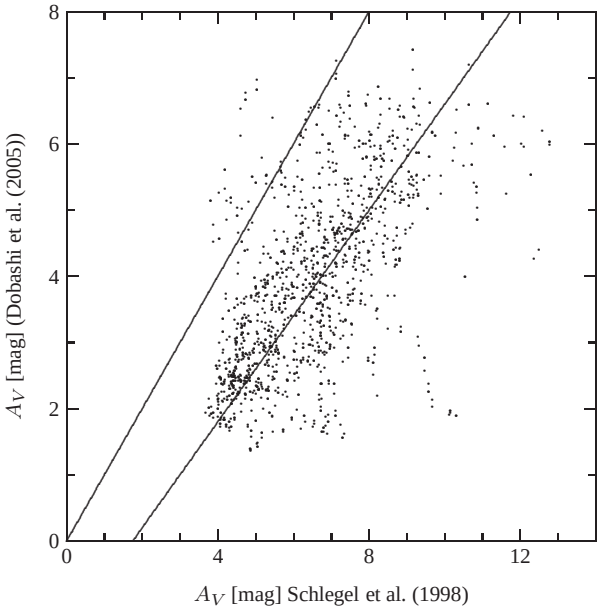

Figure A18. Comparison of the optical extinction values for region2 (Serpens) in Table 4 between the map of D05 and the map from S98. As solid line we overplot a one-to-one line, as well as a linear fit. See Table 4 for the parameters of the fit.

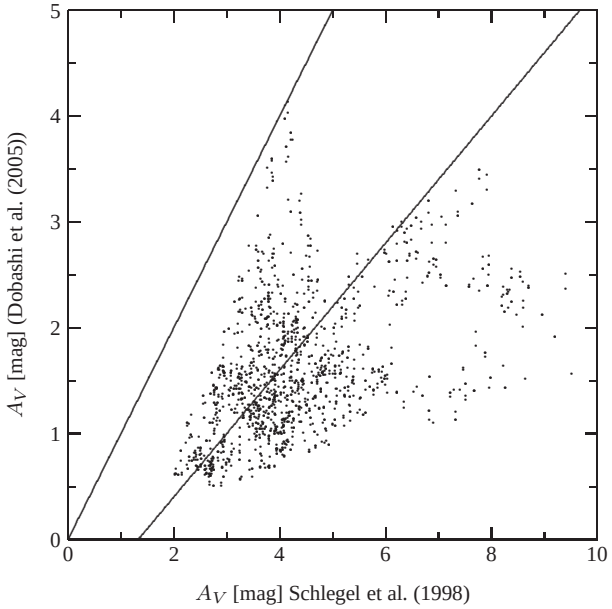

Figure A19. Comparison of the optical extinction values for region3 (Lupus) in Table 4 between the map of D05 and the map from S98. As solid line we overplot a one-to-one line, as well as a linear fit. See Table 4 for the parameters of the fit.

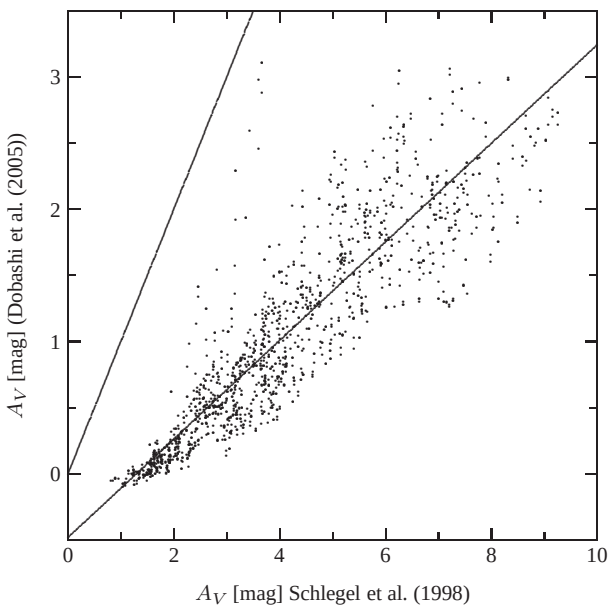

Figure A20. Comparison of the optical extinction values for region4 (Vela) in Table 4 between the map of D05 and the map from S98. As solid line we overplot a one-to-one line, as well as a linear fit. See Table 4 for the parameters of the fit.

A3 Dobashi et al. (2005) vs. Schlegel et al. (1998)

APPENDIX B: HIGH RESOLUTION A_V MAPS

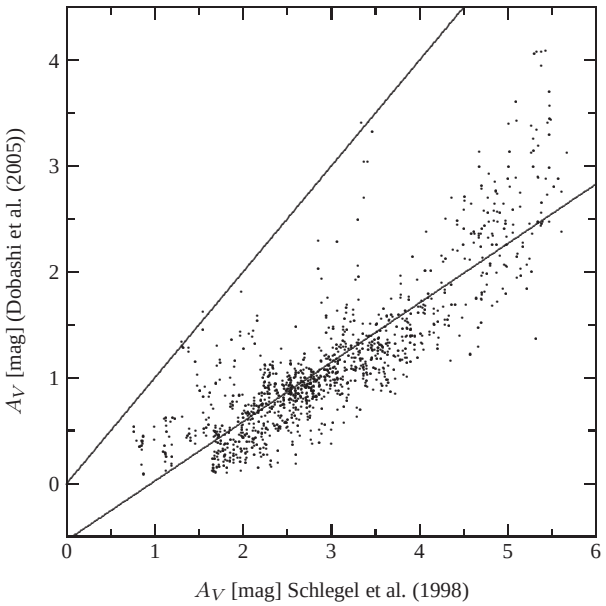

Figure A21. Comparison of the optical extinction values for region5 (Taurus) in Table 4 between the map of D05 and the map from S98. As solid line we overplot a one-to-one line, as well as a linear fit. See Table 4 for the parameters of the fit.

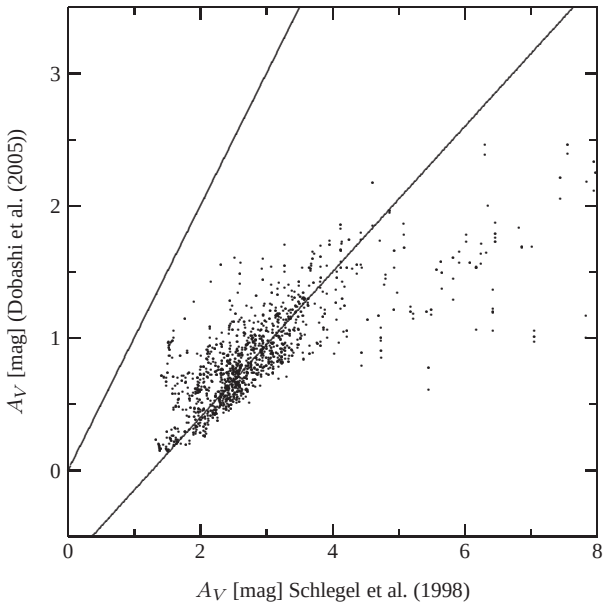

Figure A23. Comparison of the optical extinction values for region7 (Monoceros) in Table 4 between the map of D05 and the map from S98. As solid line we overplot a one-to-one line, as well as a linear fit. See Table 4 for the parameters of the fit.

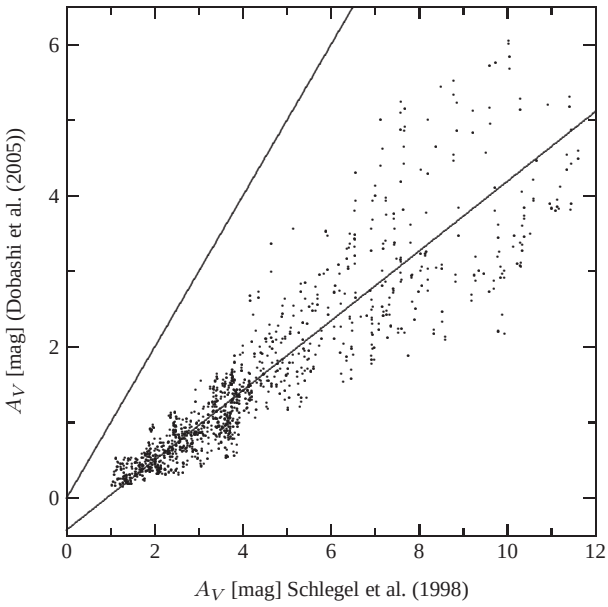

Figure A22. Comparison of the optical extinction values for region6 (North America Nebula) in Table 4 between our extinction map and the map from S98. As solid line we overplot a one-to-one line, as well as a linear fit. See Table 4 for the parameters of the fit.

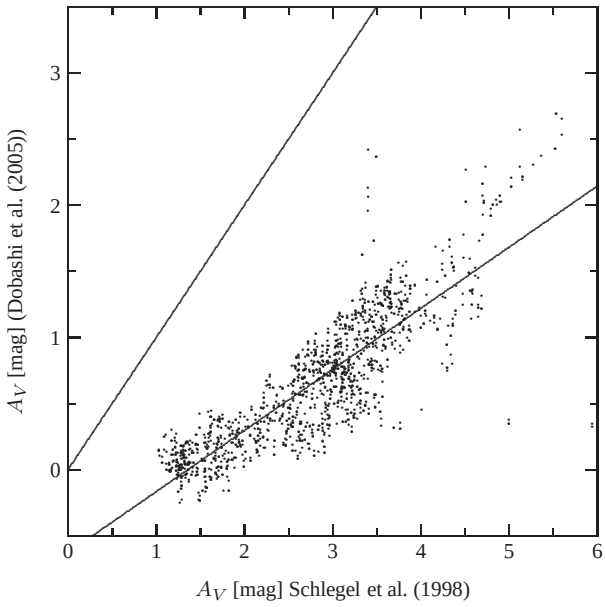

Figure A24. Comparison of the optical extinction values for region8 (Auriga) in Table 4 between the map of D05 and the map from S98. As solid line we overplot a one-to-one line, as well as a linear fit. See Table 4 for the parameters of the fit.

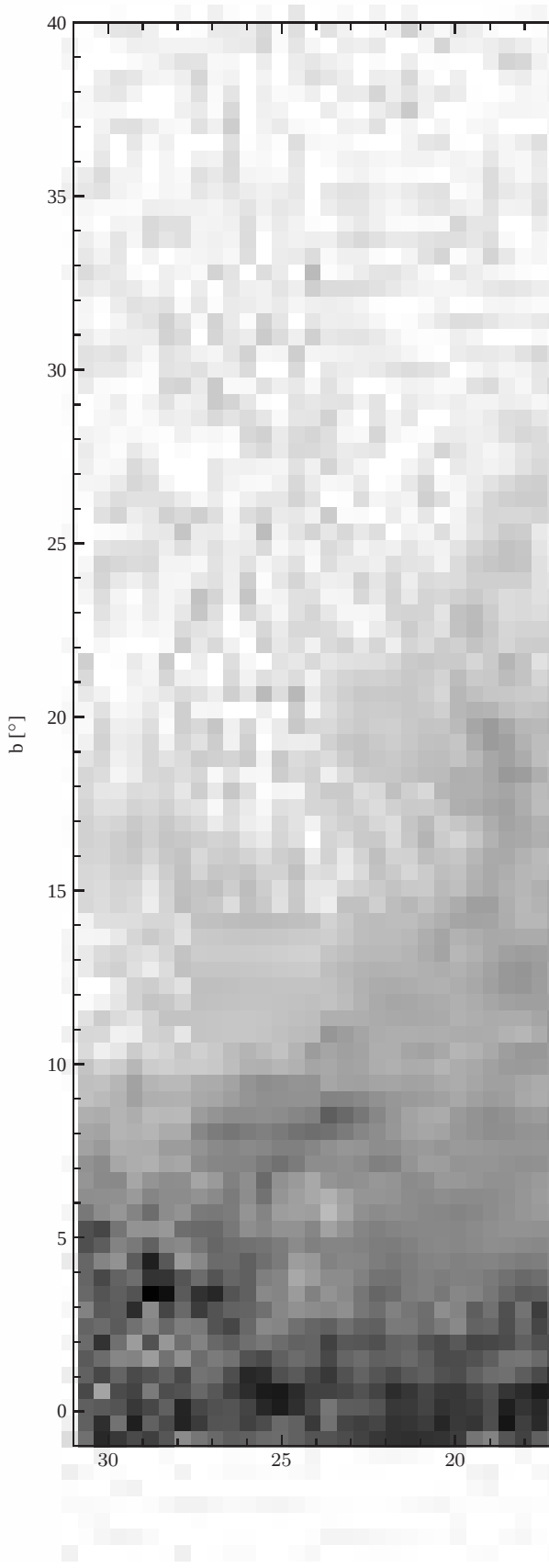
40
35
30
25
20
15
10
5
0
b [°]
30
25
20

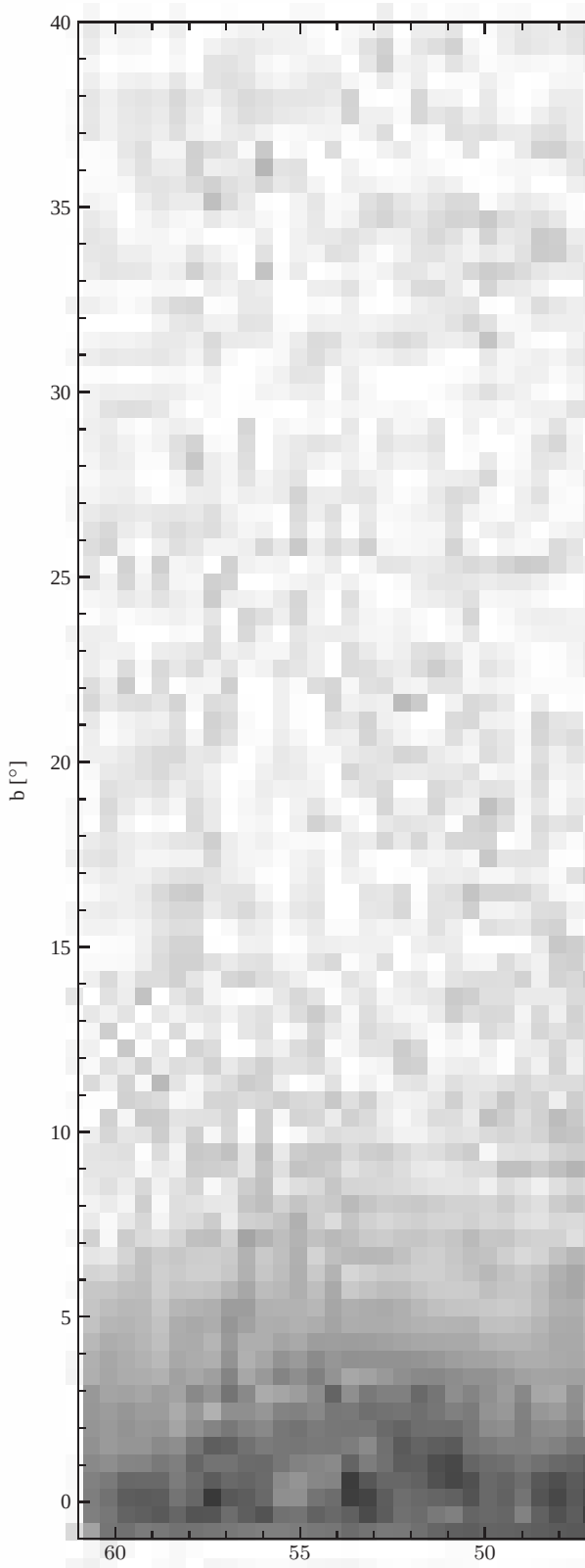
40
35
30
25
20
15
10
5
0
b [°]
60
55
50

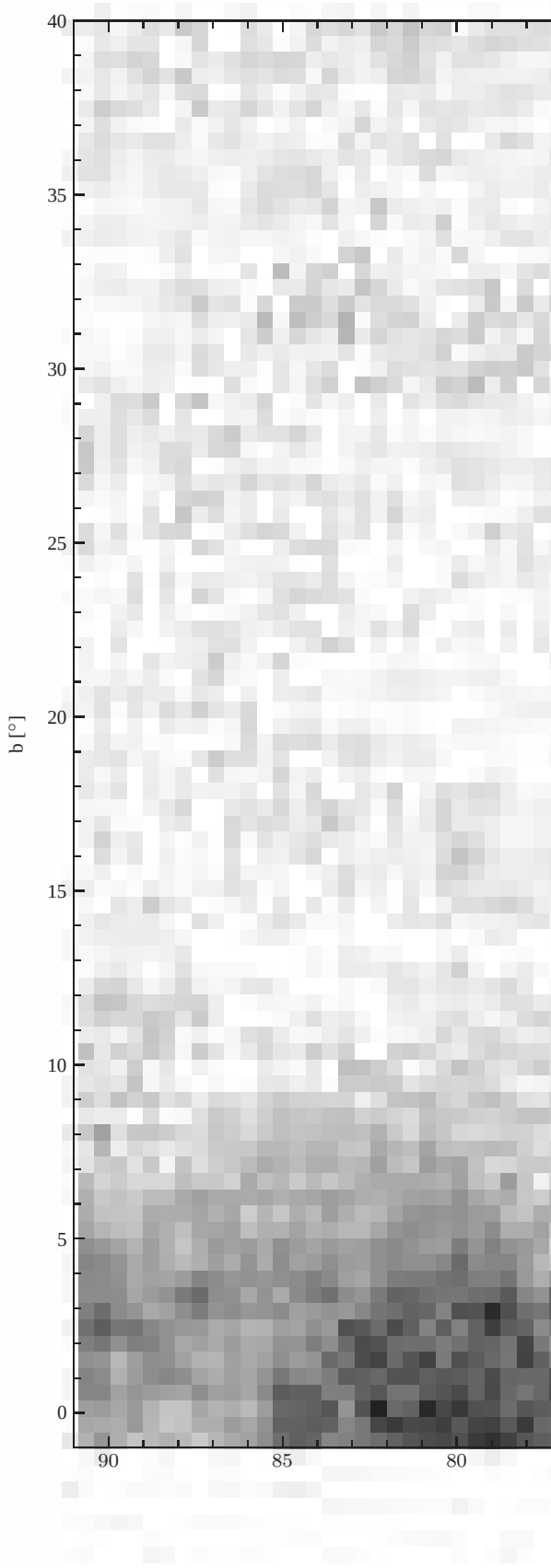
40
35
30
25
20
15
10
5
0
b [°]
90
85
80

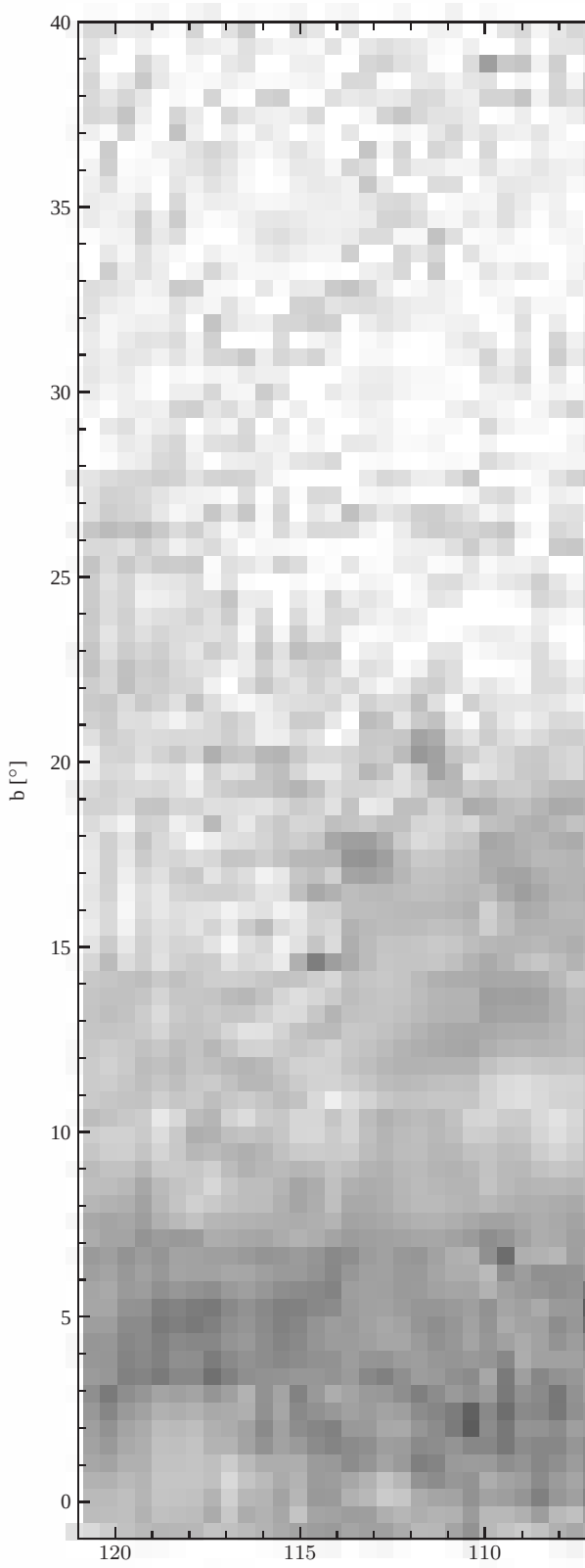
40
35
30
25
20
15
10
5
0
b [°]
120
115
110

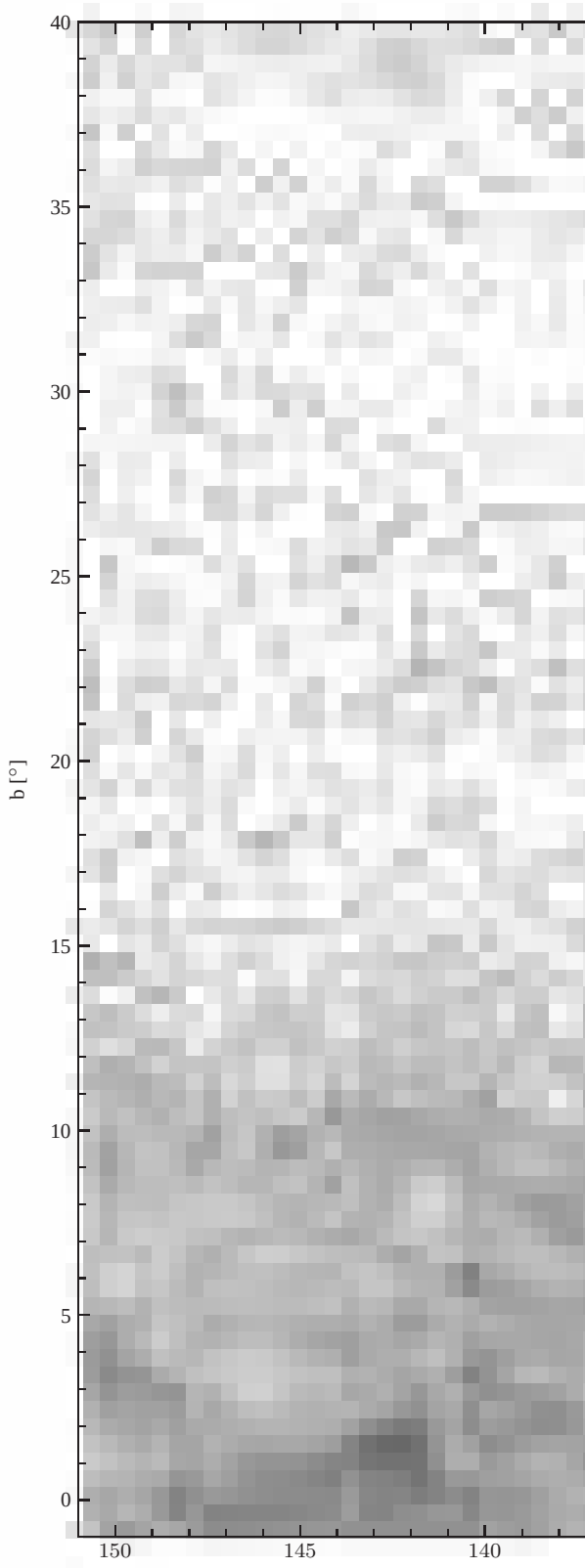
40
35
30
25
20
15
10
5
0
b [°]
150
145
140

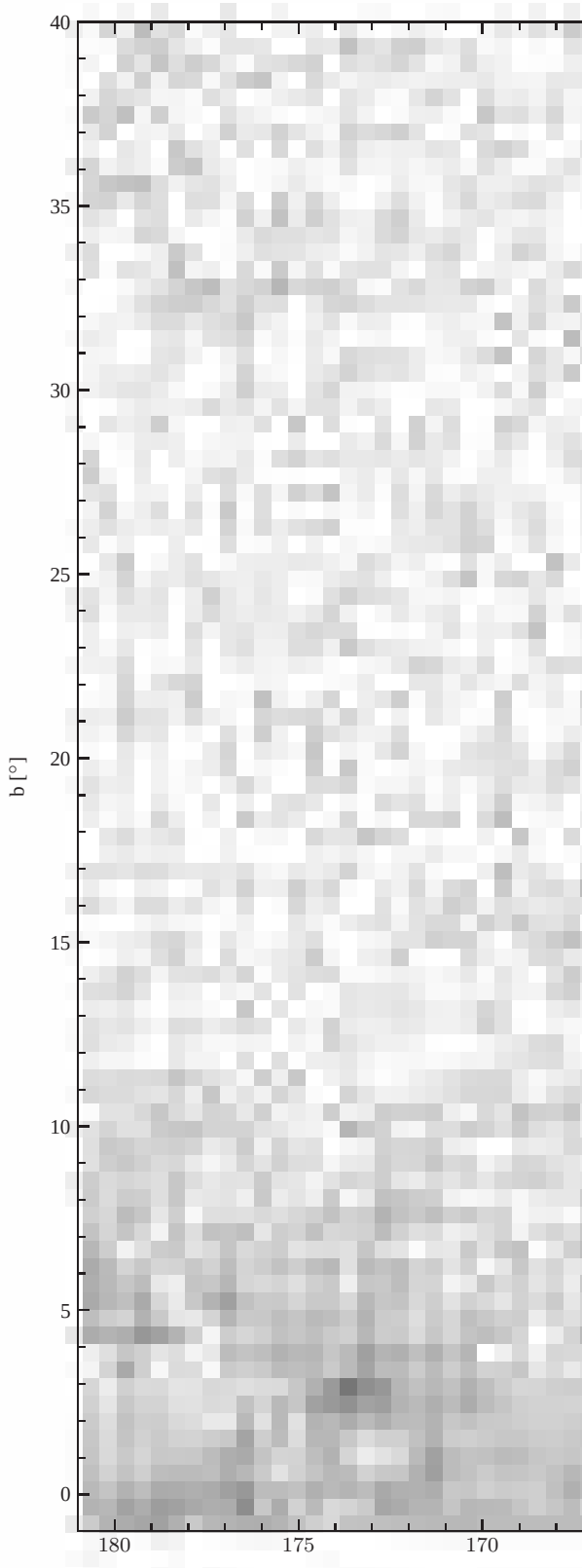
40
35
30
25
20
15
10
5
0
b [°]
180
175
170

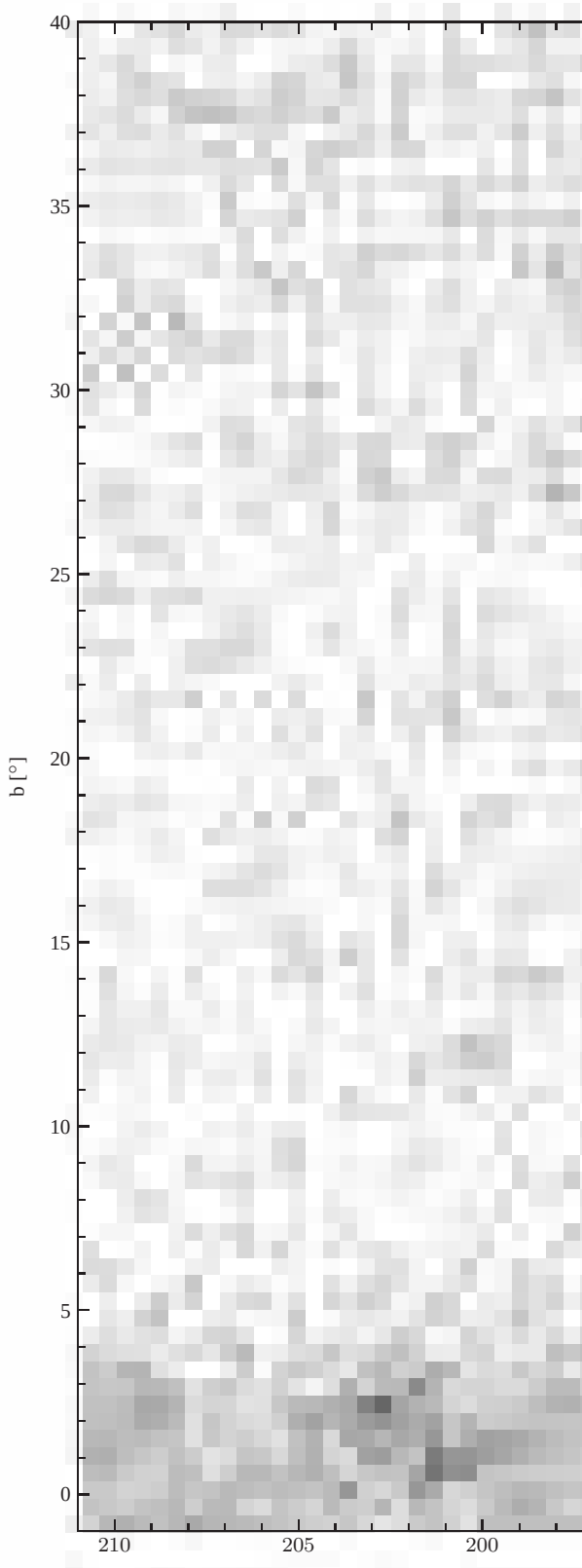
40
35
30
25
20
15
10
5
0
b [°]
210
205
200

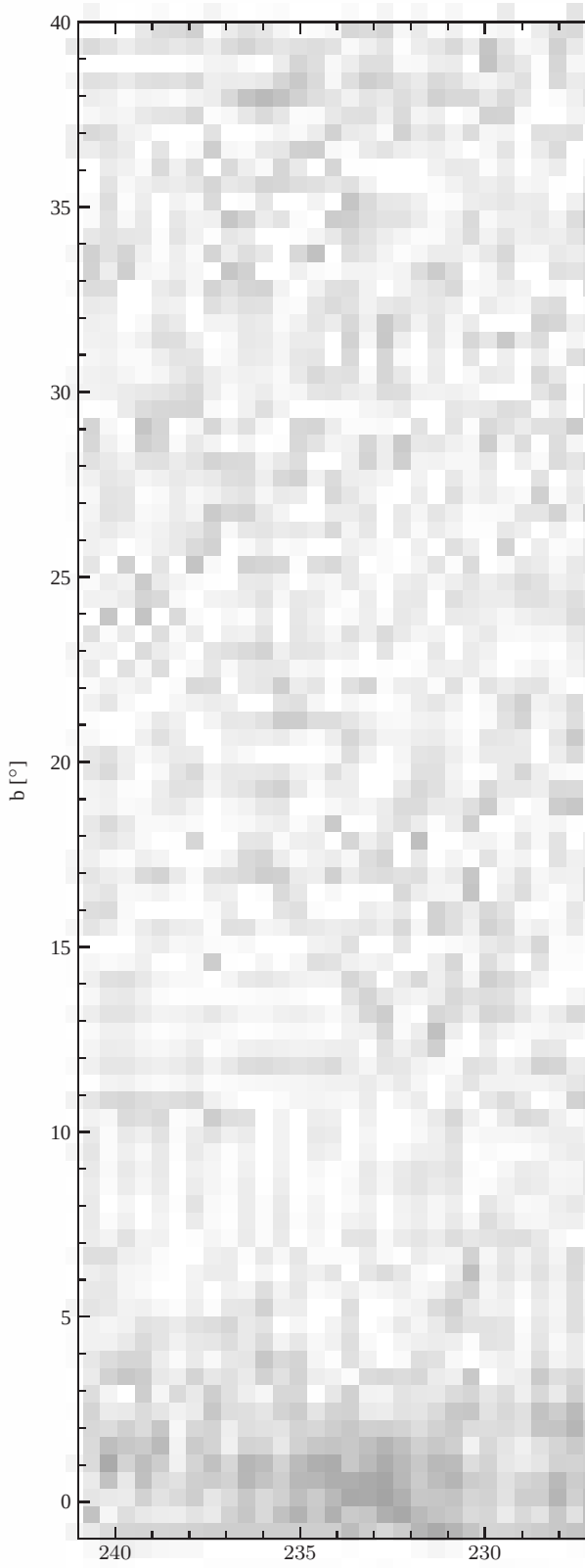
40
35
30
25
20
15
10
5
0
b [°]
240
235
230

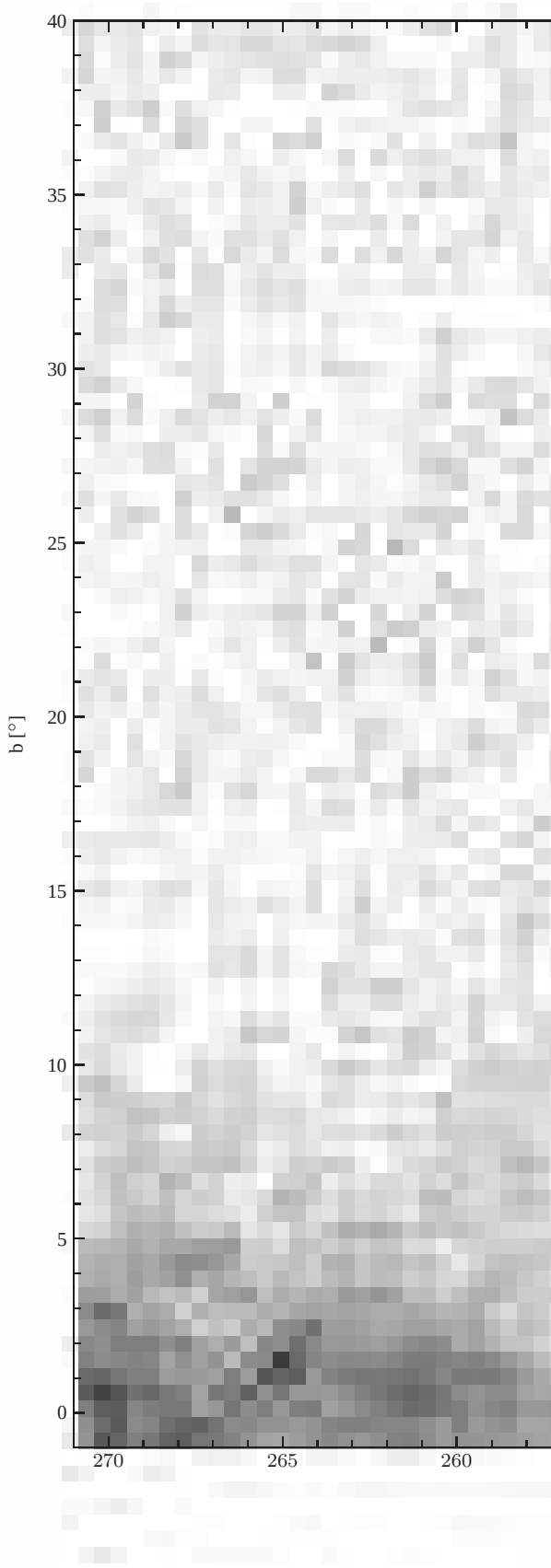
40
35
30
25
20
15
10
5
0
b [°]
270
265
260

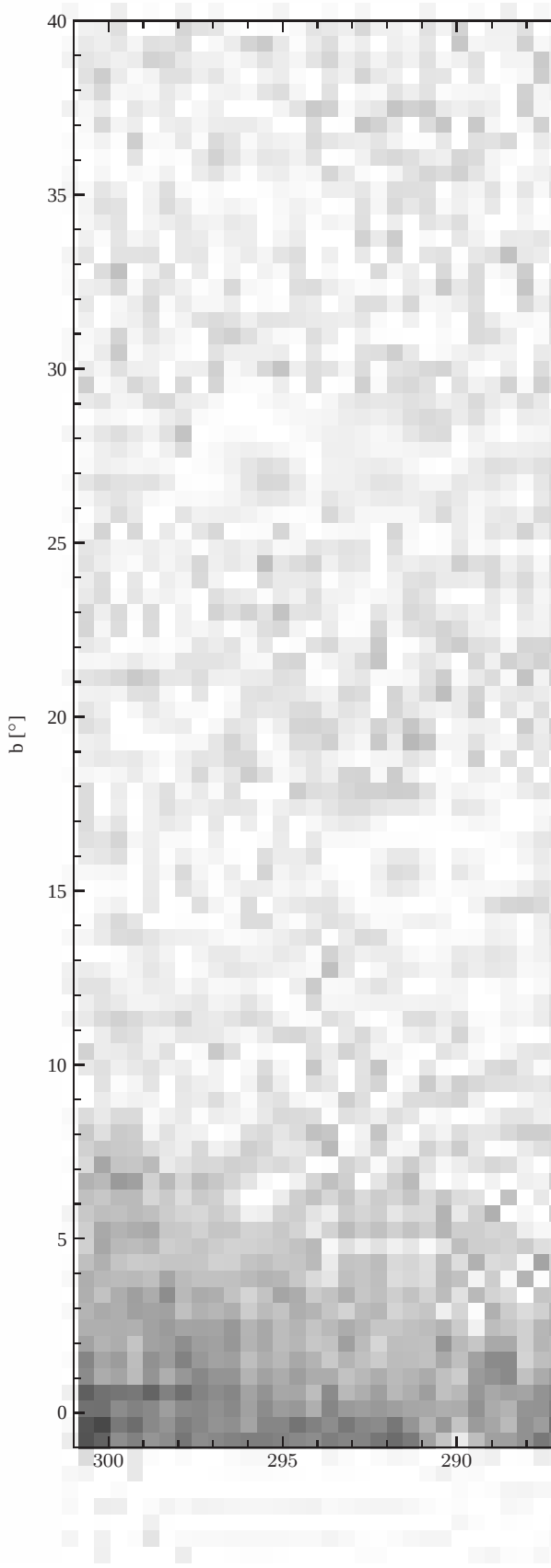
40
35
30
25
20
15
10
5
0
b [°]
300
295
290

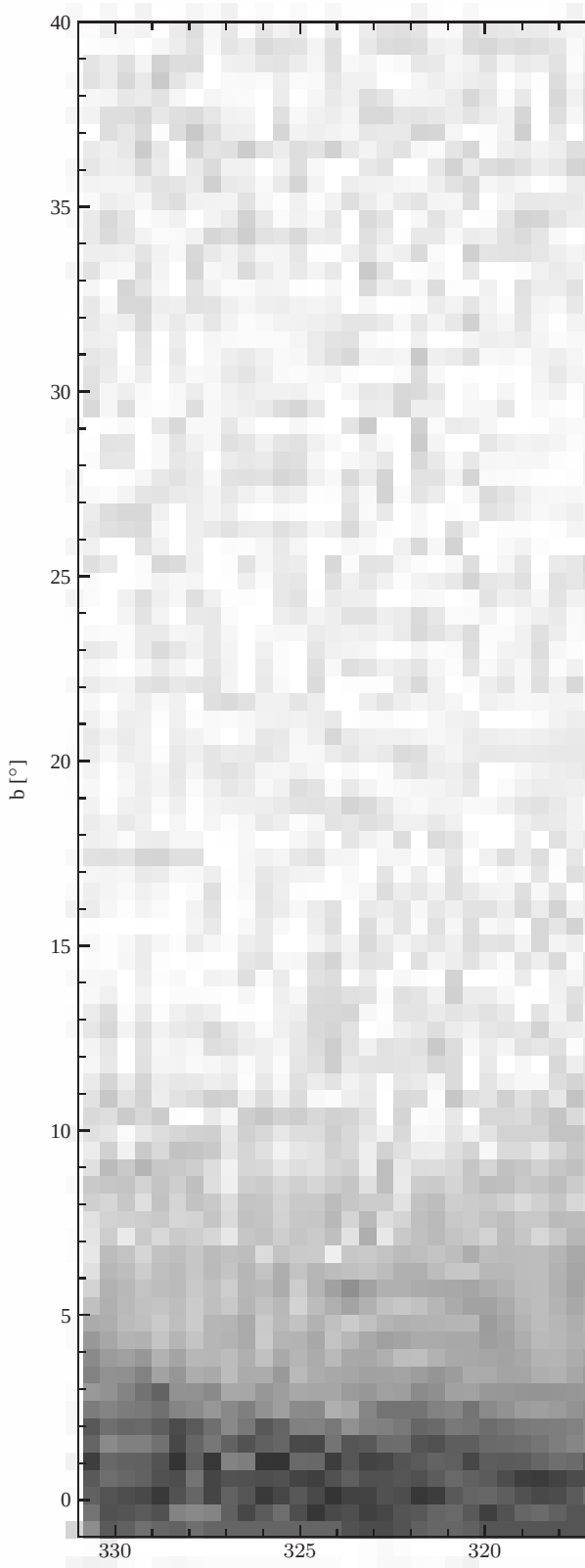
40
35
30
25
20
15
10
5
0
b [°]
330
325
320

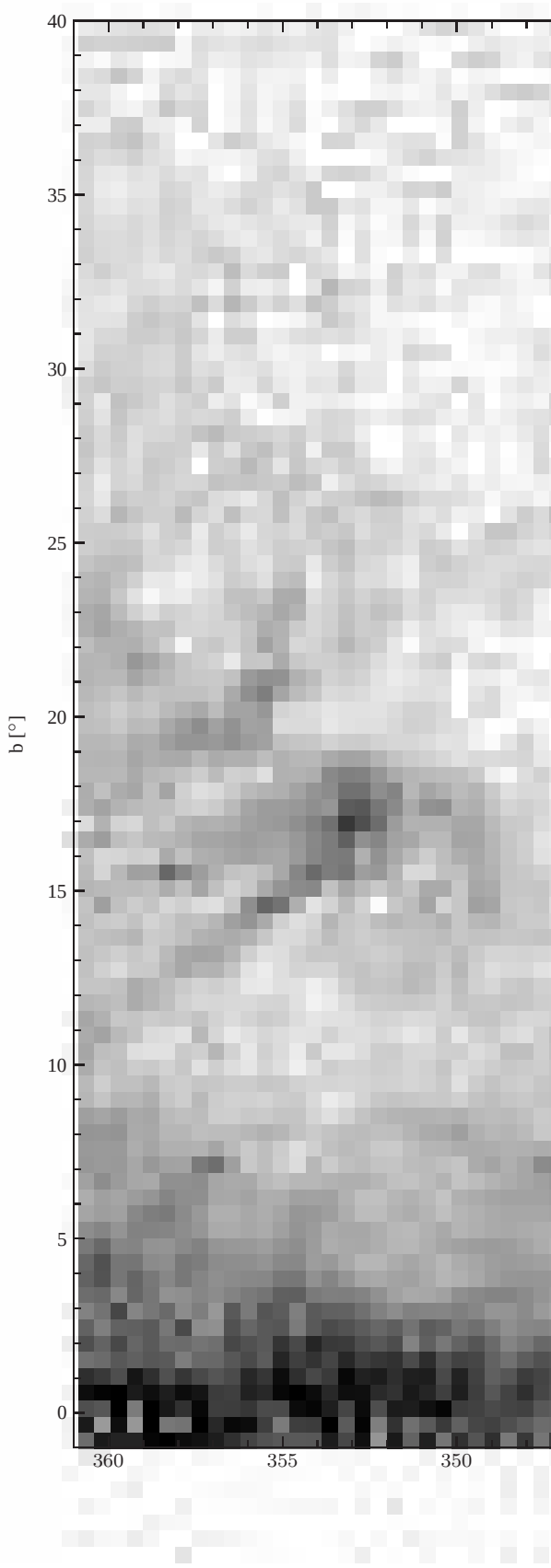
40
35
30
25
20
15
10
5
0
b [°]
360
355
350

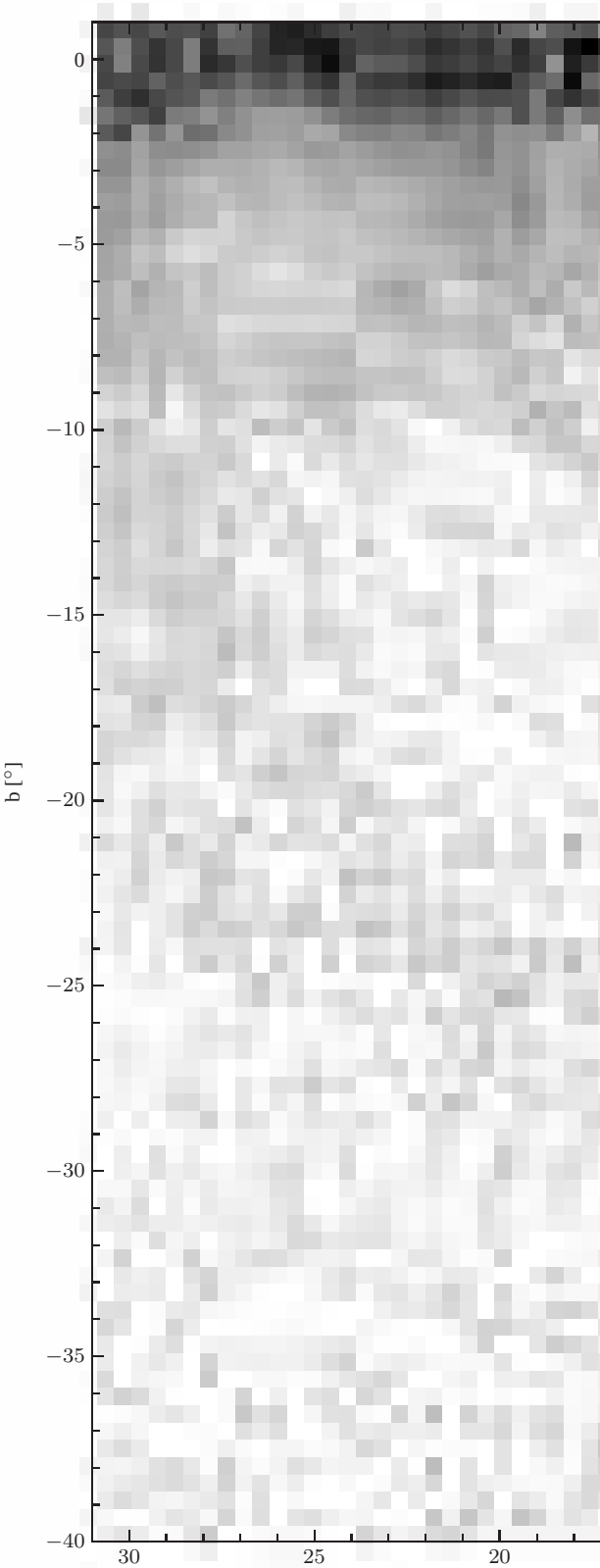
0
−5
−10
−15
−20
−25
−30
−35
−40
b [°]
30
25
20

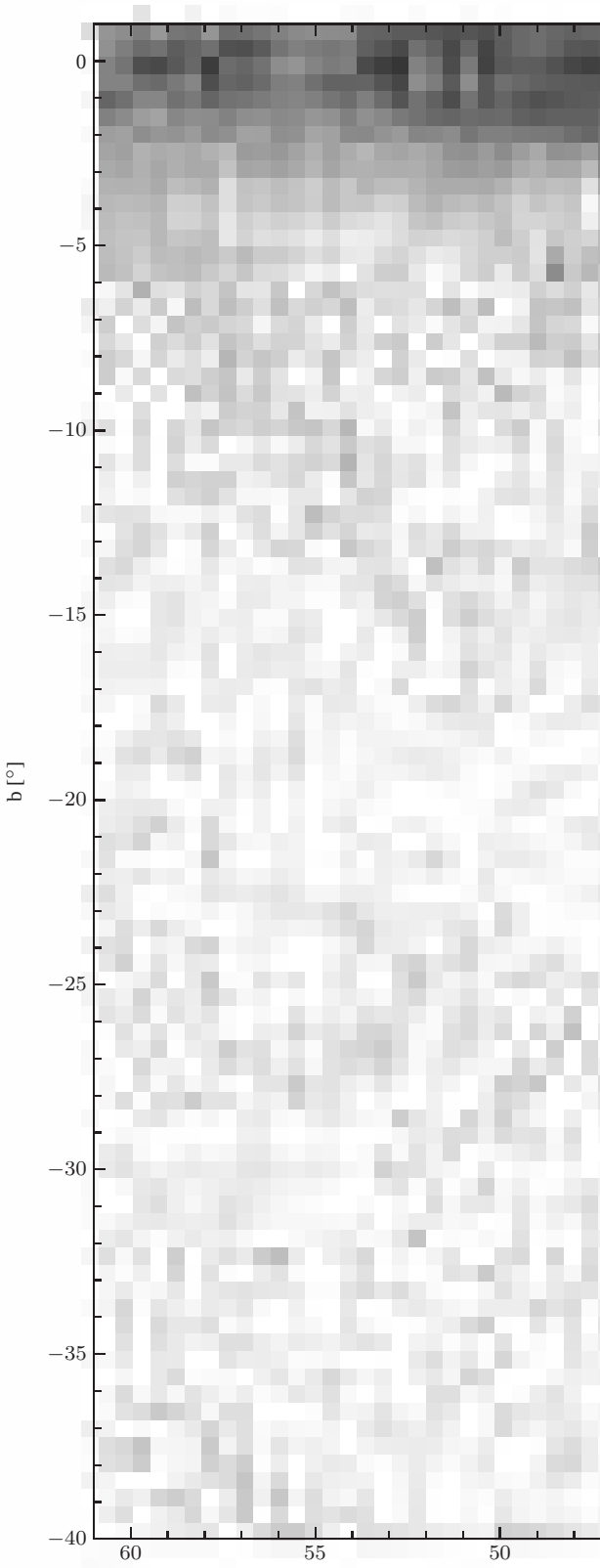
0
−5
−10
−15
−20
−25
−30
−35
−40
b [°]
60
55
50

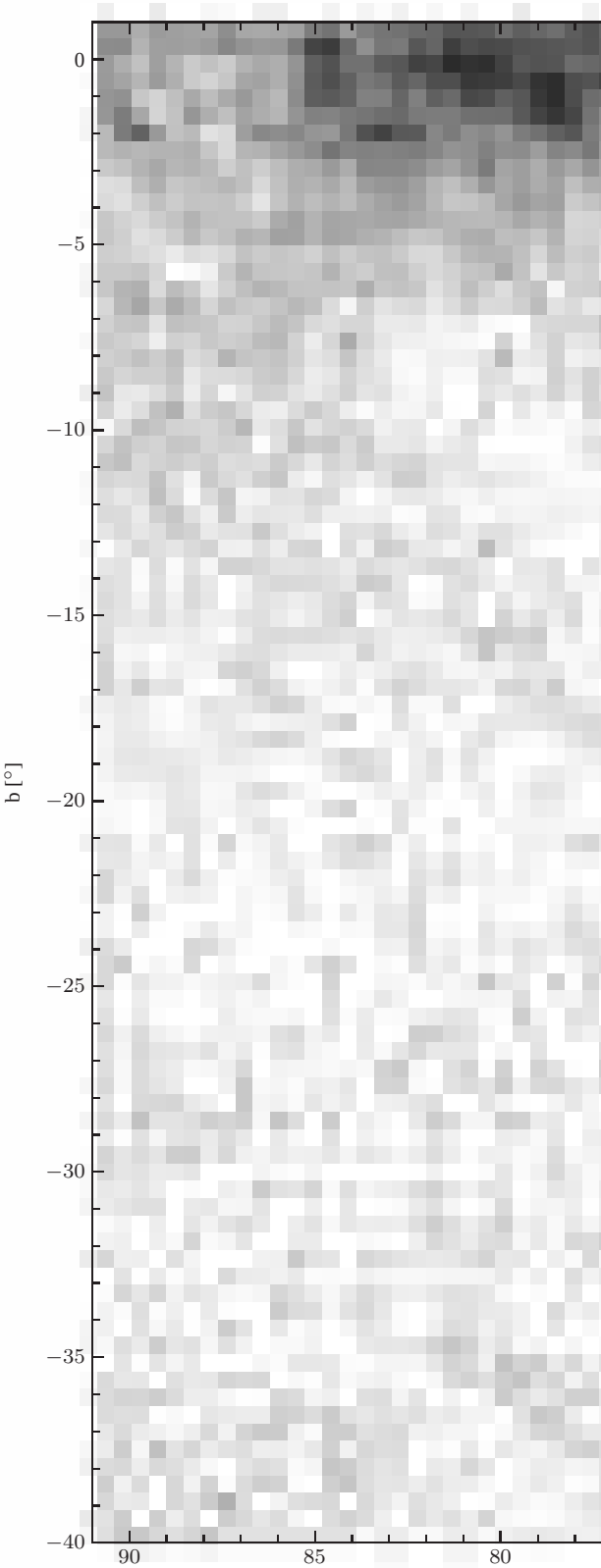
0
−5
−10
−15
−20
−25
−30
−35
−40
b [°]
90
85
80

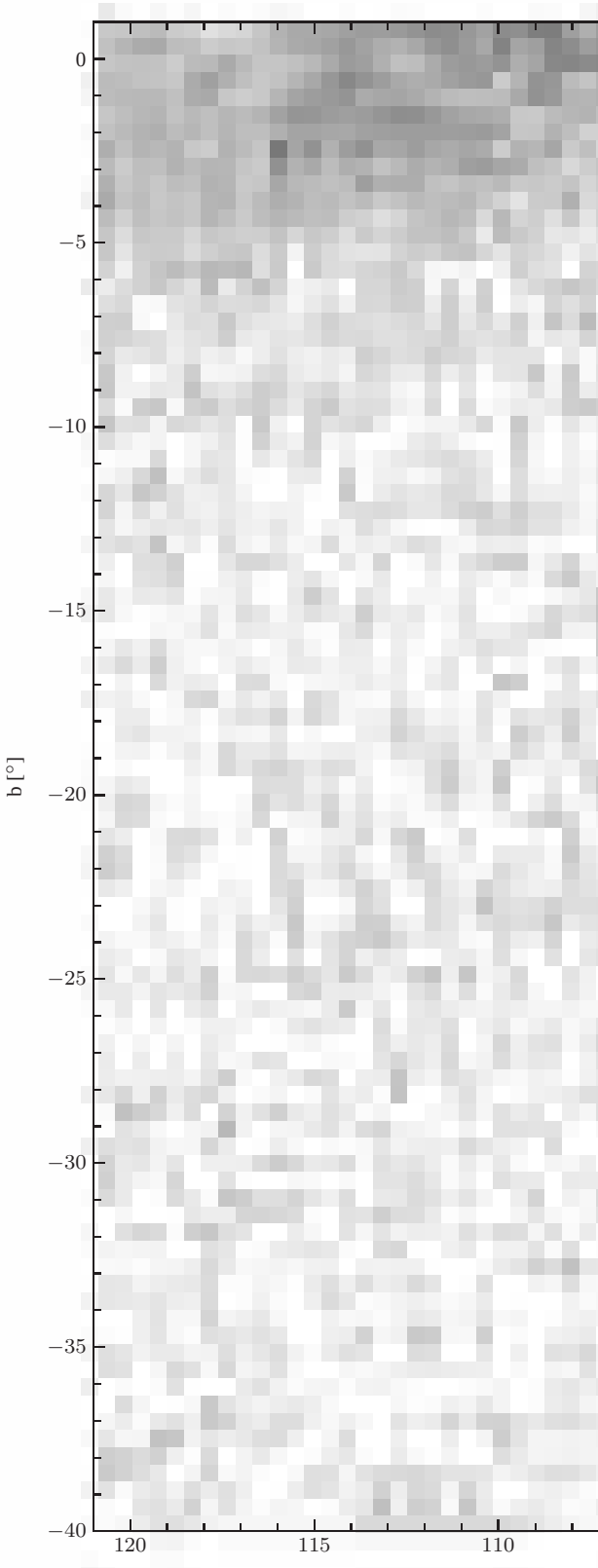
0
−5
−10
−15
−20
−25
−30
−35
−40
b [°]
120
115
110

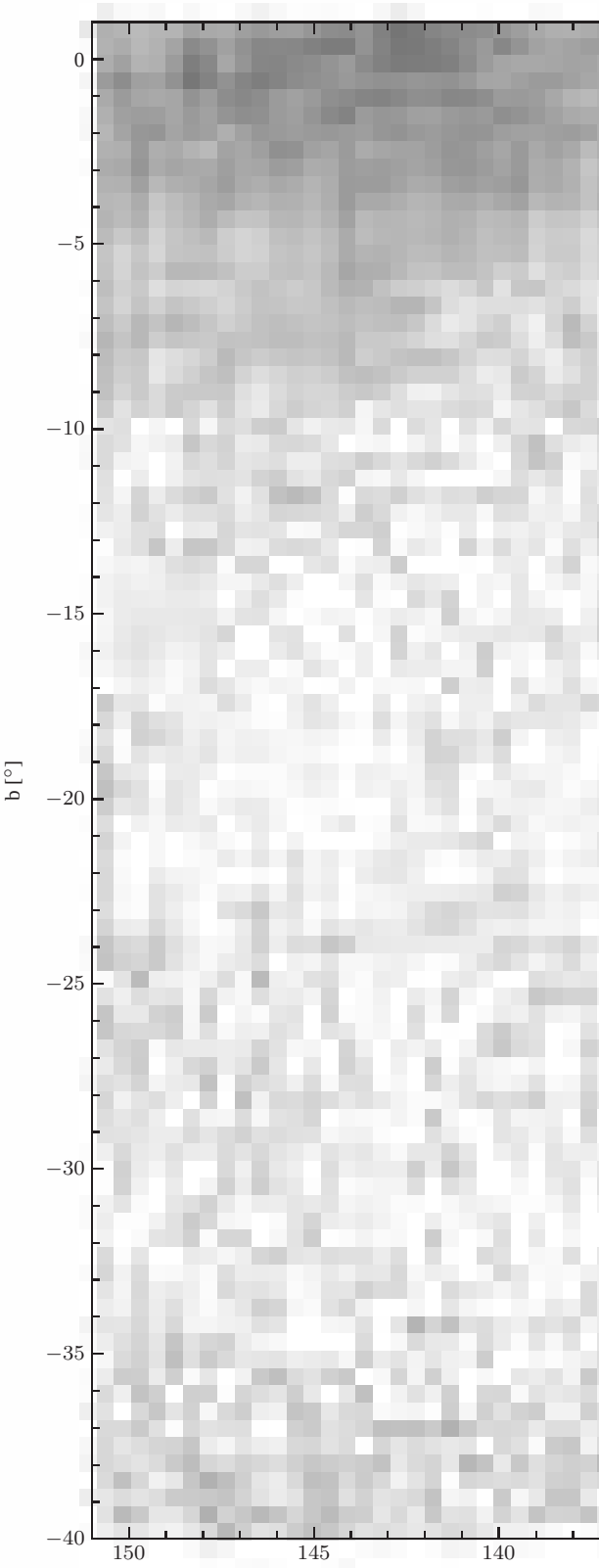
0
−5
−10
−15
−20
−25
−30
−35
−40
b [°]
150
145
140

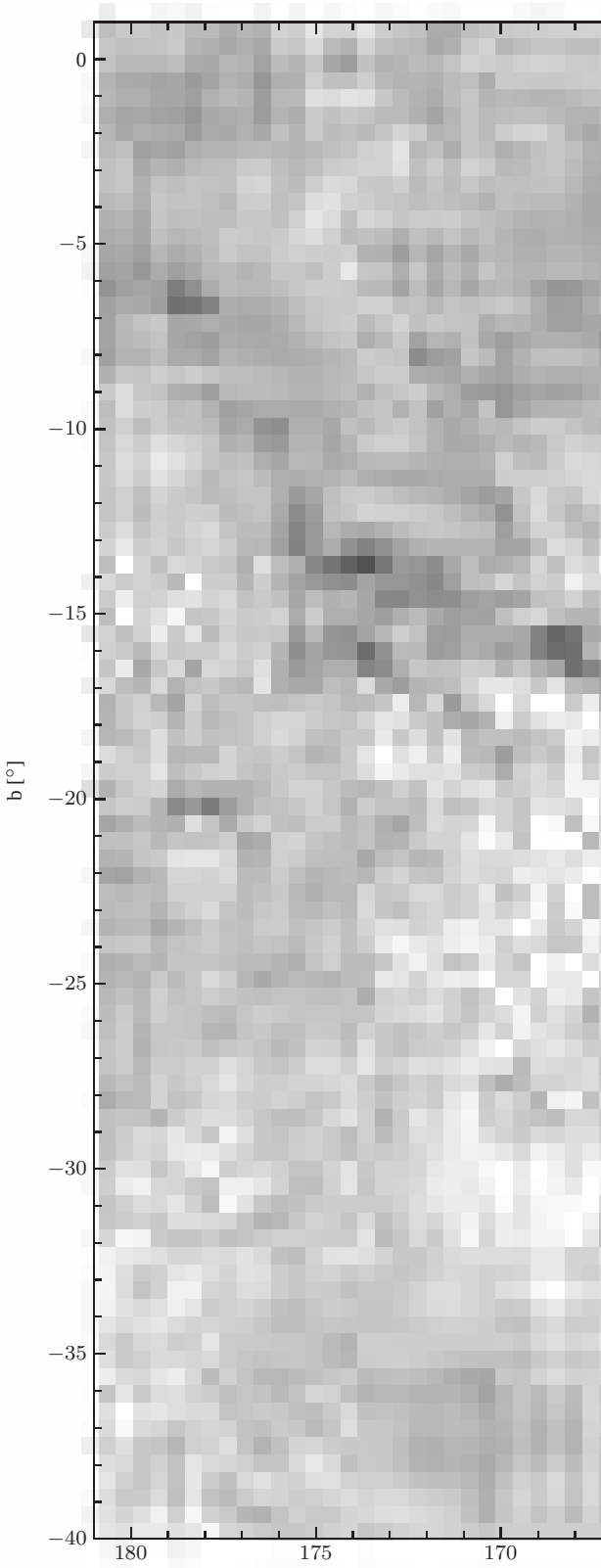
0
−5
−10
−15
−20
−25
−30
−35
−40
b [°]
180
175
170

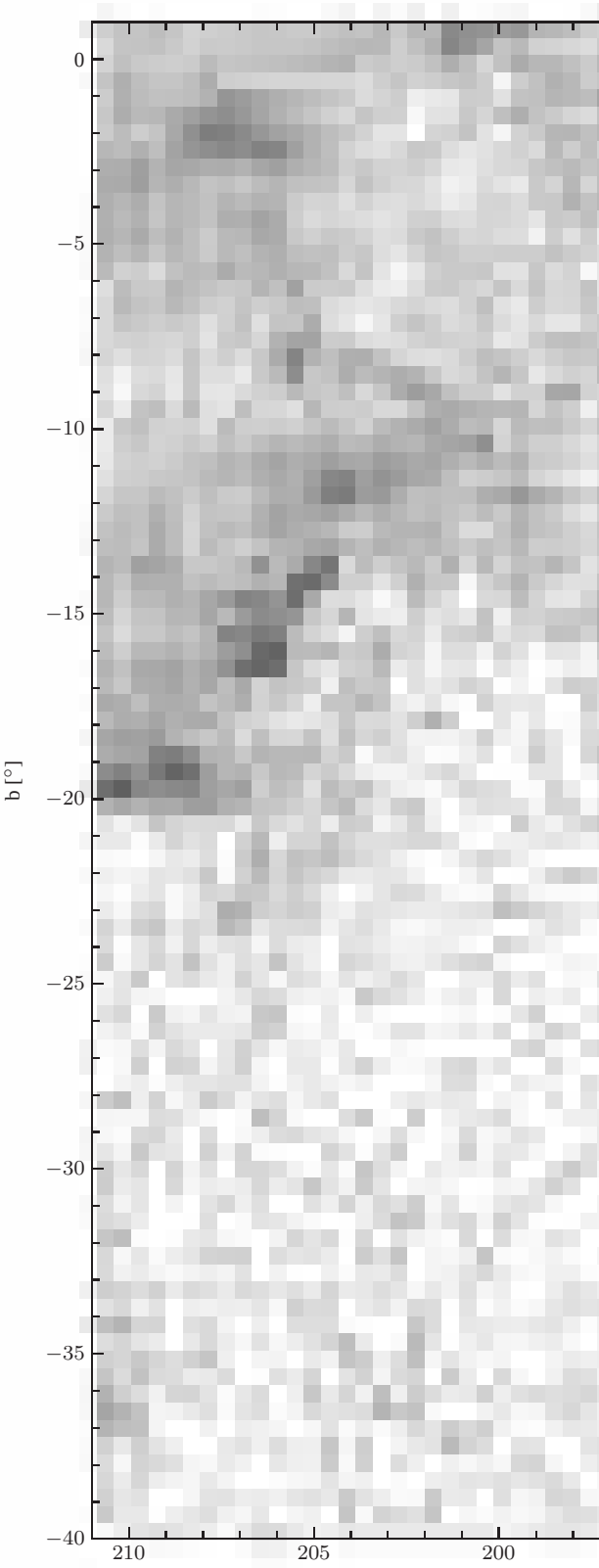
0
−5
−10
−15
−20
−25
−30
−35
−40
b [°]
210
205
200

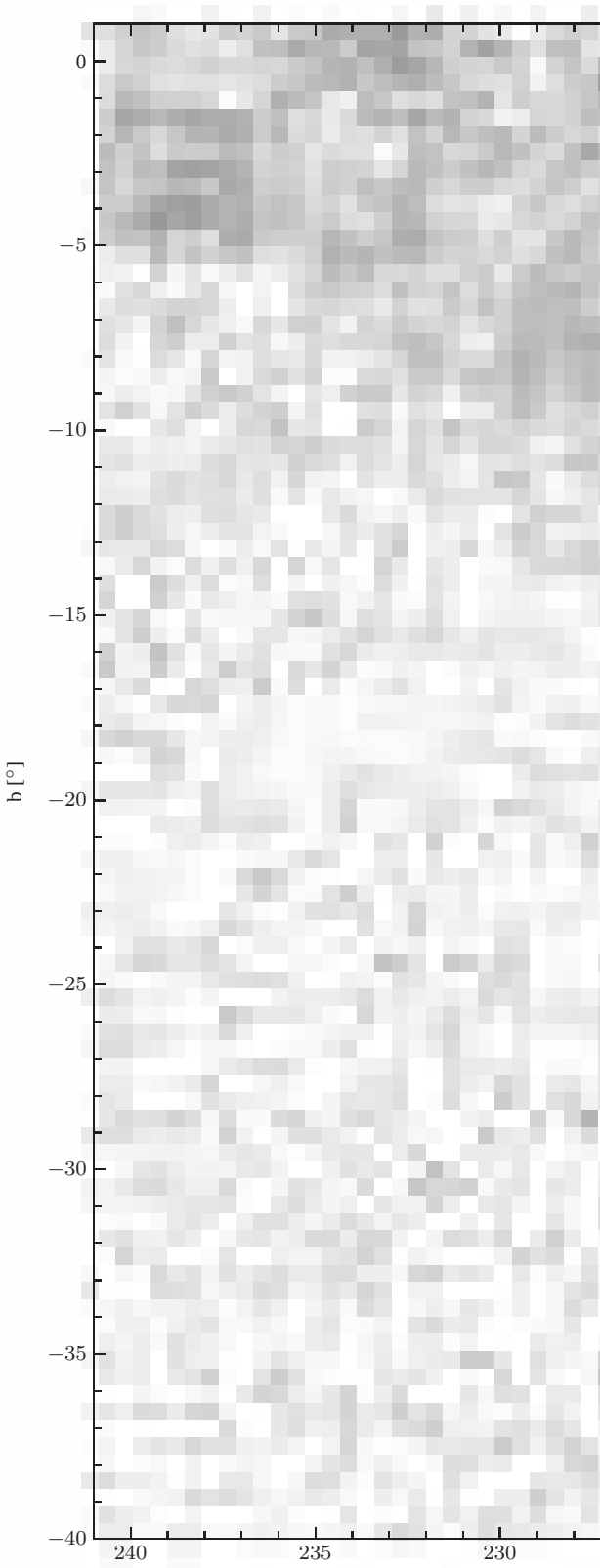
0
−5
−10
−15
−20
−25
−30
−35
−40
b [°]
240
235
230

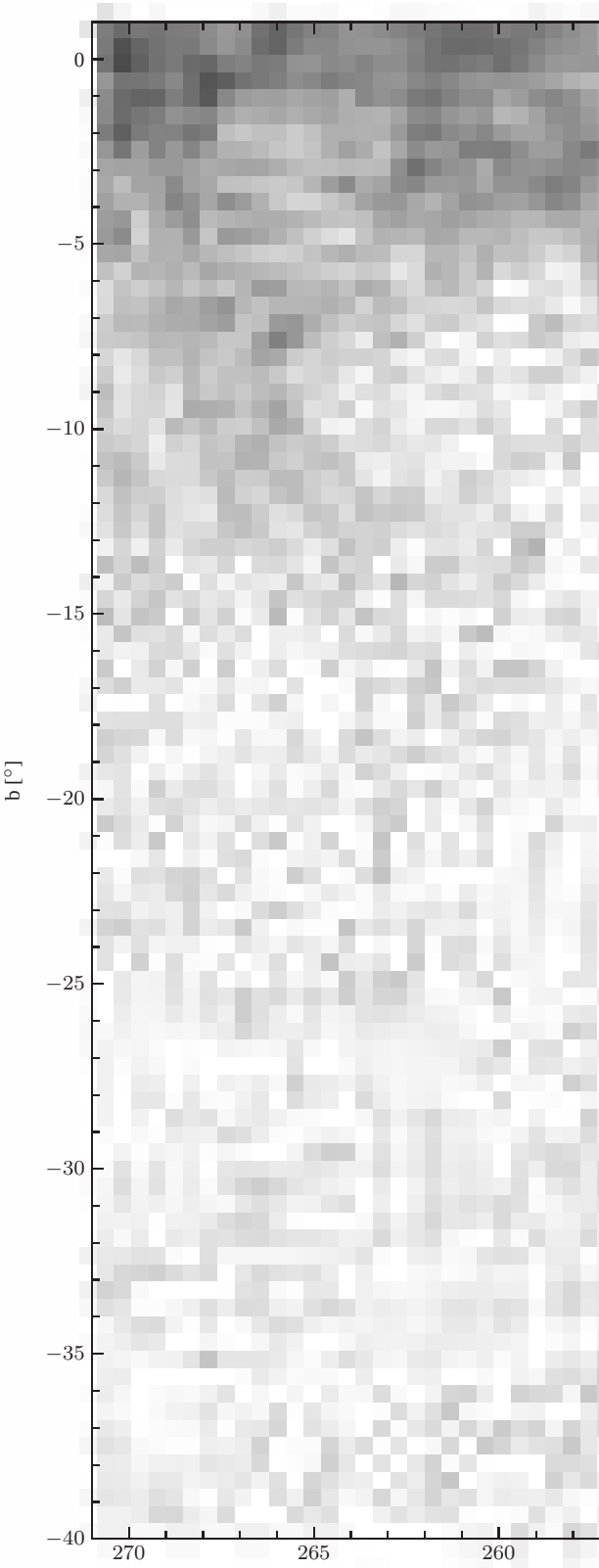
0
−5
−10
−15
−20
−25
−30
−35
−40
b [°]
270
265
260

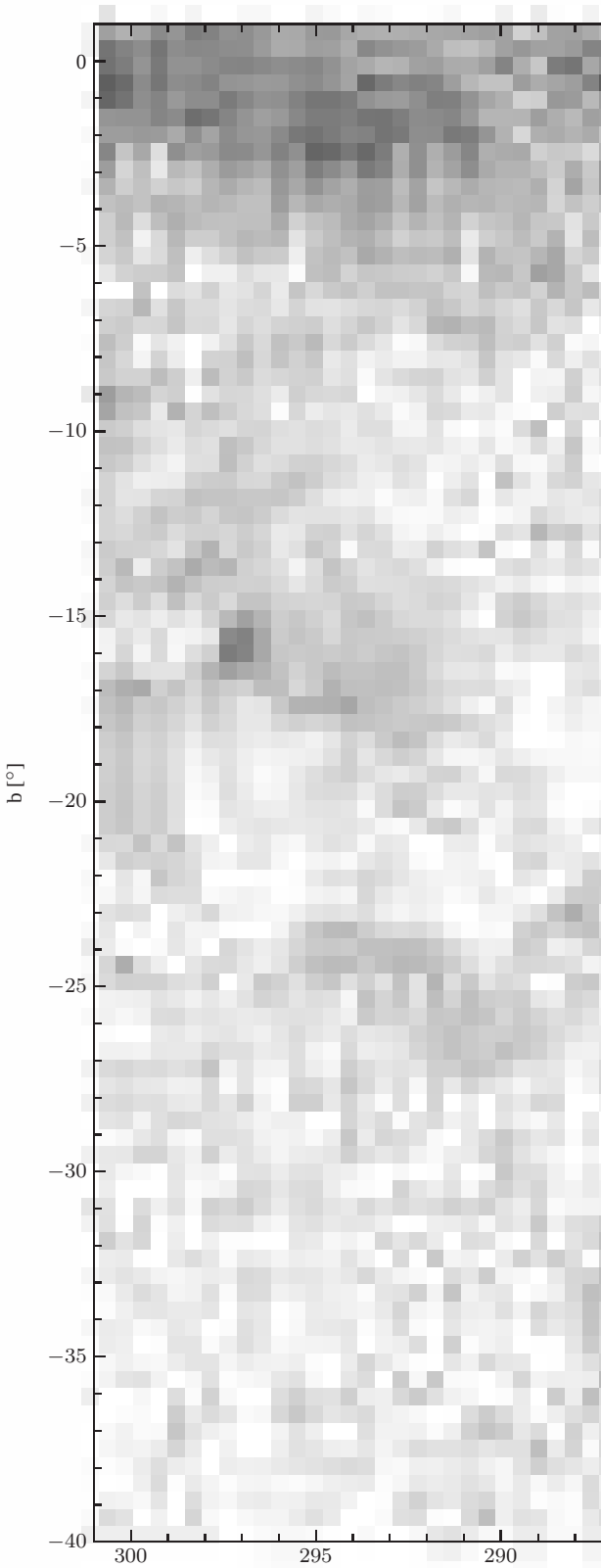
0
−5
−10
−15
−20
−25
−30
−35
−40
b [°]
300
295
290

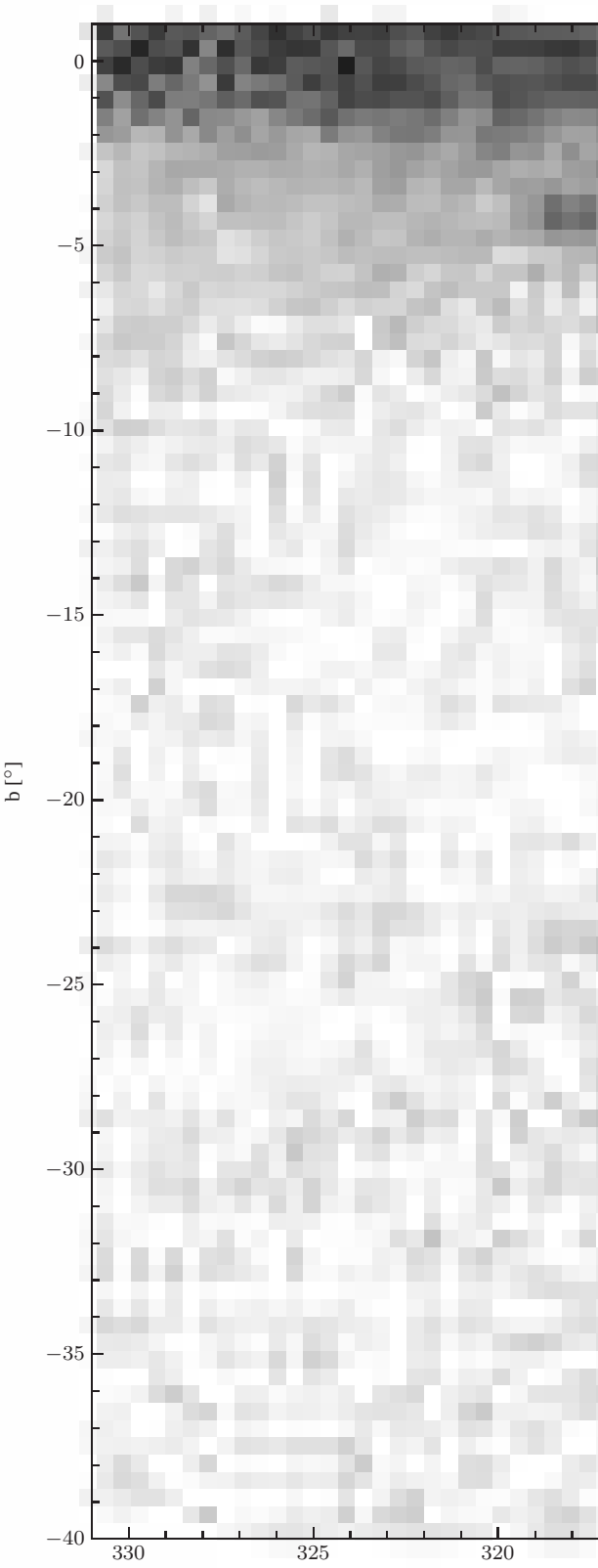
0
−5
−10
−15
−20
−25
−30
−35
−40
b [°]
330
325
320

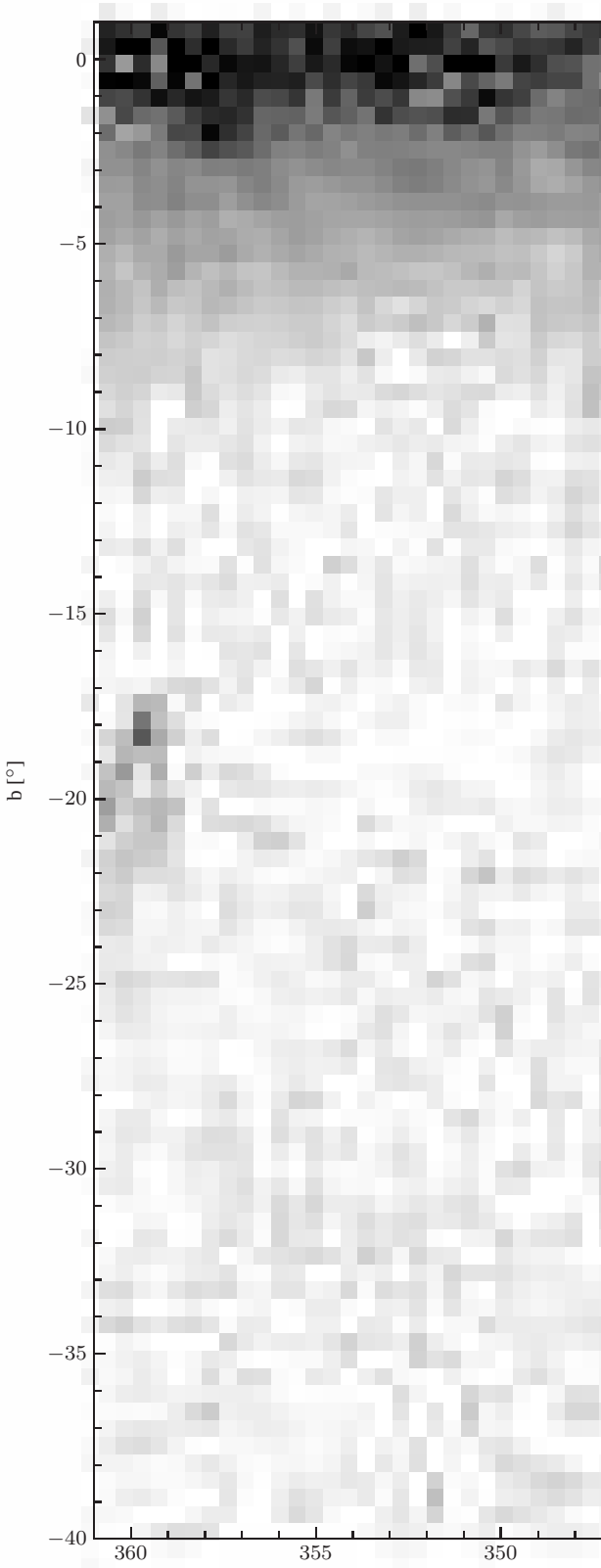
0
−5
−10
−15
−20
−25
−30
−35
−40
b [°]
360
355
350